Vpr drives massive cellular proteome remodelling in HIV-1 infection

Edward JD Greenwood[1*], James C Williamson[1*], Agata Sienkiewicz[1], Adi Naamati[1], Nicholas J Matheson[1], Paul J Lehner[1].

* These authors contributed equally to this work

1. Department of Medicine, CIMR, University of Cambridge, CB2 0XY, UK.

Corresponding Author: Paul J Lehner, pjl30@cam.ac.uk

Running title: Global effects of HIV Vpr on the cellular proteome.

Abstract

Viruses target host proteins for degradation to enhance their replication and transmission, and identifying these targets has provided key insights into the host-pathogen interaction. Here, we use complementary unbiased mass spectrometry-based approaches to dissect the widespread proteome remodelling seen in HIV-1 infected T-cells. Remarkably, the HIV accessory protein Vpr is both necessary and sufficient to cause the vast majority of these changes. This protein regulation required recruitment of the DCAF1/DDB1/CUL4 E3 ubiquitin ligase complex and the substrate binding surfaces of Vpr, but was mostly independent of Vpr mediated cell cycle arrest. Combined approaches of pulsed-Stable Isotope Labelling with Amino Acids in Cell Culture (SILAC) and immunoprecipitation-mass spectrometry (IP-MS) identified at least 38 cellular proteins directly targeted for degradation by Vpr. Thus, whilst other HIV-1 accessory proteins downregulate a small number of specific host factors, Vpr degrades multiple protein targets, causing systems-level changes to the cellular proteome. Depletion of a subset of the novel cellular targets identified in this study, including KIF18A/B, ZNF512B and ESCO2, was conserved across Vpr variants from diverse primate lentiviral lineages, confirming their biological importance *in vivo*. Further, antagonism of multiple novel Vpr targets identified here can explain previously described cellular Vpr phenotypes such as modulation of NF-κB signalling, premature chromatid segregation, and cell cycle arrest.

Significance Statement

HIV-1 encodes four 'accessory proteins', required for replication *in vivo* but not *in vitro*. The functions of three of these proteins are well characterised – they degrade a small number cellular proteins, that reflect the critical pathways HIV must antagonise to replicate within the host. The fourth accessory protein, Vpr, is much less understood. Here we show that unlike the other accessory proteins, Vpr causes hundreds of changes to the cellular proteome, by directly degrading at least 38 proteins. In fact, almost all protein-level changes that occur in an HIV infected cell require Vpr. These complex changes explain why understanding the function of Vpr has been problematic, and provide a dramatically different new context for existing and future studies of Vpr.

Introduction

The HIV-1 'accessory proteins' Vif, Vpr, Nef and Vpu deplete host proteins in infected cells, and are required for viral replication *in vivo*(1-3). We previously used unbiased quantitative proteomics to map temporal changes in cellular protein abundance during HIV infection of CEM-T4 T-cells, and identify novel targets of Vpu (SNAT1), Nef (SERINC3/5) and Vif (PPP2R5A-E)(4, 5). Nonetheless, known accessory protein targets only account for a tiny fraction of all protein changes observed

during HIV infection(5). Since a single accessory protein, Vif, is sufficient to drive global remodelling of the cellular phosphoproteome(5), we hypothesised that undiscovered targets of the final accessory protein, Vpr, might explain a proportion the remaining protein-level changes.

Results

Vpr is required for global proteome changes in HIV infected cells.

We compared total proteomes of uninfected cells with cells infected with either WT HIV or an HIV Vpr deletion mutant (HIV ΔVpr) at an infectious MOI of 1.5 (**Fig. 1a**), resulting in approximately 75% infection (**Fig. 1b**). Data from this experiment are available, together with the other proteomics datasets presented here, in **Supplementary Table 1**. As expected, amongst the 7,774 quantitated proteins, we observed widespread changes in cells infected with wild-type HIV (**Fig. 1c** left panel). Together with known Nef, Vpu and Vif, targets, we saw depletion of previously reported Vpr targets including HLTF(6, 7), ZGPAT(8), MCM10(9), UNG(10), TET2(11), MUS81 and EME1(12). DCAF1, part of the ligase complex used by Vpr to degrade targets was also depleted, consistent with a previous report (13).

In HIV ΔVpr infection (**Fig. 1c**, right panel), depletion of Nef, Vpu and Vif targets was maintained. Remarkably, as well as abolishing depletion of known Vpr targets, almost all of the previously uncharacterised protein changes were also reduced or abolished. Whilst 1,944 proteins changed significantly ($q<0.01$) in WT HIV-infected cells, only 41 protein changes retained significance when cells were infected with HIV ΔVpr. Principle component analysis confirmed that cells infected with ΔVpr virus share more similarity on the proteome level with uninfected cell than with cells infected with WT virus (**Fig. 1d**).

Incoming Vpr protein alone drives massive cellular proteome remodelling.

Since Vpr enhances expression of other viral proteins(14, 15) (**Fig 1c**), differences between WT and ΔVpr viruses could potentially be explained by secondary changes in expression levels of these proteins, or different rates of progression of WT and ΔVpr viral infections. To eliminate these confounders, we repeated our proteomic analysis using cells exposed to lentiviral particles lacking or bearing Vpr in the presence of reverse transcriptase inhibitors (RTi), thus excluding all *de novo* viral protein expression (**Fig. 2a**). Cells were exposed to these viral particles at an infectious MOI of 0.5, determined in the absence of RTi.

Strikingly, changes induced by Vpr-containing viral particles phenocopied the Vpr-dependent changes seen in HIV infection (**Fig. 2b**), with a high degree of correlation (**Fig. 2c**). Taking both experiments together, Vpr is therefore both necessary and sufficient for the significant ($q<0.01$) depletion of at least 302 proteins, and the upregulation of 413 – highlighted in blue and red, respectively (**Fig. 2c**). This is a stringent false discovery rate and, in practice, the number of Vpr-dependent changes is almost certainly even higher. Where antibodies were available, we confirmed a proportion of these changes by immunoblot (**Supplementary Fig. S1**).

Cellular proteome remodelling requires interaction with DCAF1 and cellular substrates.

Vpr is found in all primate lentiviruses, but its function or functions remain controversial. Nonetheless, in all phenotypic descriptions, Vpr activity is dependent on the interaction between Vpr and the DCAF1/DDB/Cul4 ligase complex, recruitment of which results in degradation of known

Vpr targets through the ubiquitin-proteasome system. The Q65 residue of Vpr is required for the interaction with DCAF1(16), and we therefore compared proteome changes caused by a Q65R Vpr mutant with changes caused by WT Vpr. As expected, Q65R Vpr was almost completely inactive (**Fig. 2d,e,**).

We recapitulated this finding by comparing the effects of WT Vpr in control cells, or cells depleted of DCAF1 using RNAi (**Fig. 2f**). All changes were reduced in magnitude in the DCAF1 knockdown cells (**Fig. 2g**), which showed an approximately 50% reduction in levels of DCAF1 (**Supplementary Fig. 2**). As with depletion of known Vpr targets, extensive Vpr-dependent proteomic remodelling is dependent on the interaction between Vpr and DCAF1.

Like Q65, residues E24, R36, Y47, D52 and W54 of Vpr are required for the recruitment and degradation of previously reported Vpr targets, and are thought to form the substrate binding surface(7, 17). In particular, Y47, D52 & W54 are hypothesized to be crucial to a proposed DNA mimicking motif used to bind the known Vpr target UNG2(17). Accordingly, the $Vpr_{E24R, R36P}$ and Vpr_{W54R} mutants were somewhat attenuated in their ability to cause proteome remodelling, and a triple mutant, $Vpr_{Y47A, D52A, W54R}$, was defective for almost all Vpr-dependent protein changes (**Fig. 2d,e** see also **Supplementary Fig. 3**).

Vpr causes G2/M arrest in cycling cells, but the mechanism for this is contentious(18, 19), as is the connection, if any, to the replicative advantage Vpr provides *in vivo*. Previous datasets have identified proteins increased or depleted during different phases of the cell cycle or in G2/M arrested cells(20, 21) (**Supplementary Fig. 4**). As expected, regulation of the cyclin family of proteins during the G2 and M phases of cell is recapitulated by Vpr (**Supplementary Fig. 4b**). Whilst some changes in protein levels induced by Vpr may therefore be explained by the effects of cell cycle arrest, proteins regulated by cell cycle in these datasets only account for a small fraction of Vpr-dependent changes (**Supplementary Fig. 4a,c,d**).

Further, residue S79 of Vpr is specifically required for Vpr-dependent cell cycle arrest(22), confirmed by our finding that Vpr_{S79A} was unable to cause cell cycle arrest (**Fig 2d** and **Supplementary Fig. 3**). Additionally, Vpr_{Q65R} and $Vpr_{Y47A, D52A, W54R}$ mutants are also unable to cause G2/M arrest, while $Vpr_{E24R, R36P}$ has an intermediate phenotype, and Vpr_{W54R} caused G2/M arrest at wild type levels. Strikingly, most Vpr-dependent protein changes were also observed with the Vpr_{S79A} mutant (**Fig. 2d,e**), and are therefore independent of G2/M cell cycle arrest. The presence or absence of G2/M arrest was also a poor correlate of proteomic remodelling caused by the other mutants. Cell cycle arrest therefore only explains a minority of Vpr-dependent changes.

Identifying direct targets for Vpr mediated degradation.

Cellular proteins may be regulated directly or indirectly. We previously proposed candidate direct Vpr targets by identifying proteins downregulated during WT HIV infection with similar temporal expression profiles to UNG and HLTF[5]. As predicted, most of these proteins were significantly reduced in abundance by Vpr in this study (**Supplementary Fig. 5**). Strikingly, analysis of the 302 proteins depleted by Vpr (but not the proteins increased by Vpr) revealed a profound enrichment (>60%) for proteins that reside in the nucleus, and bind nucleic acid (**Supplementary Fig. 6**). Previously reported direct Vpr targets are all nuclear proteins, and Vpr associates with DNA binding proteins such as UNG via a substrate-binding surface that mimics DNA (17). Rather than targeting a

122 small number of cellular proteins for degradation, Vpr may therefore have a much wider range of
123 direct cellular targets, and this mechanism of substrate recruitment suggests a plausible structural
124 explanation.

125 To identify proteins targeted directly by Vpr, we first adopted a co-immunoprecipitation approach
126 (**Supplementary Fig. 7a**). Factors specifically co-immunoprecipitated in the presence of Vpr are
127 expected to include direct Vpr targets and, accordingly, were enriched for proteins depleted (rather
128 than increased) in the presence of Vpr (**Supplementary Fig. 7b,d,e**). Nonetheless, the co-IP was
129 dominated by DCAF1, a stable binding partner of Vpr, identified with a signal intensity 2 orders of
130 magnitude greater than all other proteins (**Supplementary Fig. 7c**). This mismatch suggests why MS-
131 IP may be more successful in identifying cellular components of stable accessory protein complexes,
132 rather than cellular targets degraded by accessory proteins, which interact transiently and in
133 competition with each other (23, 24).

134 We therefore adopted an alternative, pulsed SILAC approach to identify host proteins specifically
135 destabilised within 6 hrs of exposure to Vpr (**Fig. 3a**). Since proteins are fully labelled prior to
136 exposure to Vpr, differences in abundances of labelled proteins between conditions exclusively
137 reflect changes in protein degradation rates. This technique is directly analogous to a traditional
138 pulse-chase experiment using radiolabelled methionine/cysteine, but allows a global, unbiased
139 analysis of potential cellular targets(25).

140 Six hours after exposure to Vpr, the stability of most proteins was unchanged (**Fig. 3b**). However, a
141 subset of proteins depleted by Vpr were already destabilised, consistent with Vpr-dependent
142 proteasomal degradation. These 27 proteins, including HLTF, are therefore very likely to represent
143 direct targets for Vpr-mediated depletion (**Fig. 3c**). After 24 hours of exposure to Vpr, changes in
144 protein stability reflected overall changes in protein abundance caused by Vpr in other experiments
145 (**Fig. 3b**), including proteins with increased as well as decreased stability. These changes are
146 therefore indicative of both direct and indirect Vpr targets.

147 Combining these two orthogonal approaches, we have identified 38 direct targets for Vpr mediated
148 degradation (Fig. 3d). Vpr is both necessary and sufficient for depletion of these proteins, which are
149 either bound by Vpr, or destabilised within 6 hours of Vpr exposure (or both). This list very likely
150 underestimates the true number of direct Vpr targets, as several known targets of Vpr behaved
151 appropriately, but beyond the statistical cut-offs used to derive this table (**Supplementary Table 2**).
152 It is also limited to proteins expressed in this T-cell model.

153 **Conservation of Vpr targets across primate lentiviruses.**
154 Targeting of key cellular proteins such as BST2 or the APOBEC3 family is conserved across multiple
155 lentiviral lineages, demonstrating the *in vivo* selective advantage of these interactions. We therefore
156 tested a diverse panel of lentiviral Vpr proteins for shared activity with the NL4-3 Vpr variant used in
157 all the experiments above. We included Vpr variants from primary isolates of HIV-1 from two distinct
158 cross-species transmissions from apes to humans (Group M and Group O), in addition to a closely
159 related SIVcpz variant. We also tested Vpr variants from divergent primate lineages, including HIV-2,
160 SIVsmm, SIVagm and SIVrcm (**Fig. 4a** and **Supplementary Fig. 8**). Since depletion of some substrates
161 switches between Vpr and Vpx, in lineages bearing this accessory gene, we also included a Vpx
162 variant from HIV-2.

163 Extensive Vpr-dependent remodelling of the cellular proteome was conserved across the HIV-
164 1/SIVcpz lineage (**Fig. 4b**,**c**). Vpr variants from other lineages showed a narrower set of changes, but
165 some proteins, particularly those most heavily depleted by HIV-1, were targeted by Vpr variants
166 across multiple lineages (**Fig. 4b**,**c,d**). Depletion of selected proteins for which commercial antibody
167 reagents were available was confirmed by immunoblot of cells transduced with an overlapping panel
168 of Vpr variants (**Fig. 4e**). Conserved targets of direct Vpr-mediated degradation (highlighted in **Fig.**
169 **4d** and **Supplementary Fig. 8c**) are likely to provide an *in vivo* replicative advantage for all primate
170 lentiviruses, while depletion of others depends on HIV-1/SIVcpz specific factors or are species
171 specific.

172 While none of the identified HIV-1 Vpr targets were degraded by Vpx, we did identify a shared ability
173 of Vpx and SIVagm Vpr to deplete TASOR, a critical component of the Human Silencing Hub (HuSH)
174 complex(26) (**Fig 4f**). This represents only the second known target of Vpx, in addition to
175 SAMHD1(27). We have previously shown that the HuSH complex mediates position-dependent
176 transcriptional repression of a subset of lentiviral integrations, and antagonism of HuSH is able to
177 potentiate HIV reactivation in the J-LAT model of latency(26). As predicted, Vpx-VLPs phenocopied
178 the effect of RNAi-mediated TASOR depletion on reactivation of the HuSH-sensitive J-LAT clone A1
179 (**Fig. 4g**).

180 Most primate lentiviruses can be categorised into 5 lineages (**Supplementary Fig. 8a**), of which two
181 encode Vpx which degrades SAMHD1. Two lineages lack Vpx, but use Vpr to degrade SAMHD1, while
182 the HIV-1/SIVcpz lineage lacks SAMHD1 antagonism(28). We considered that TASOR antagonism
183 may follow the same pattern, and thus tested Vpx proteins from both Vpx bearing lineages, and
184 representative Vpr variants from lineages that use Vpr to degrade SAMHD1. All of these proteins
185 were able to deplete TASOR in Vpx/Vpr transduced cells (**Fig. 4h**). Antagonism of SAMHD1 and
186 TASOR therefore follow the same pattern. Whilst this manuscript was in preparation, two other
187 groups independently discovered Vpx-mediated depletion of TASOR(29, 30), and the role of HuSH
188 antagonism in lentiviral infection is the subject of ongoing investigation.

189 Discussion

190 Proteomic analyses of cells infected with viruses from different families have revealed widespread
191 and varied changes to the cellular proteome (5, 31-33). While these changes are presumed to be
192 multifactorial, in the case of HIV-1 infection, the majority can be attributed to the action of a single
193 viral protein, Vpr, a surprising result that may be mirrored in other systems. Mechanistically,
194 depletion of proteins with nucleic acid binding properties is consistent with known structural
195 determinants of Vpr substrate recruitment. From the functional viewpoint, while HIV-1 has three
196 accessory proteins (Vpu, Nef and Vif) to aid viral replication and counteract host defences in the late
197 stages of the viral life cycle, Vpr is the only HIV-1 accessory protein specifically packaged in virions.
198 Multiple targets may therefore be required both to protect incoming virions from cellular factors,
199 and to prime newly infected cells for productive viral replication.

200 Despite its importance *in vivo*, an *in vitro* viral replication phenotype is often absent in T-cell
201 infection models(34). Nonetheless, expression of Vpr in T-cells causes cell cycle arrest(35, 36), cell
202 death(36), transactivation of the viral LTR(35), enhancement or antagonism of crucial signalling
203 pathways including NFAT(37) and NF-κB(38-40), disruption of PARP1 localisation(37, 40), defects in
204 chromatid cohesion(41) and induction of the DNA damage response(42, 43). Nonetheless, the

205 molecular mechanisms underpinning these phenomena have remained elusive. Our data now reveal
206 how diverse Vpr-dependent cell biological phenotypes, at least some of which can be segregated(36,
207 37), may be underpinned by dysregulation of multiple different proteins. Critically, knockdown or
208 inhibition of numerous proteins depleted by Vpr have been independently associated with these
209 effects (summarised in **Supplemental Table 3**). Antagonism of multiple proteins results in the same
210 phenotype, with synergistic or redundant effects, while depletion of other single proteins can
211 phenocopy more than one Vpr associated phenotype.

212 Thus, Vpr degrades multiple cellular targets, resulting in global remodeling of the host proteome,
213 and labyrinthine changes to different cellular pathways. This explains why its effects on viral
214 replication are complex and remain poorly understood, why the functional consequences of
215 individual Vpr targets identified and studied in isolation have proved elusive, and why the search for
216 a single, critical Vpr target has been problematic.

217 Acknowledgements

218 This work was supported by the Wellcome Trust (PRF 101835/Z/13/Z to PJL), the MRC (CSF
219 MR/P008801/1 to NJM), NHSBT (WPA15-02 to NJM), the NIHR Cambridge BRC, and a Wellcome
220 Trust Strategic Award to the CIMR. The authors thank Dr. Reiner Schulte and the CIMR Flow
221 Cytometry Core Facility team, and the Lehner laboratory for critical discussion.

222 Author Contributions

223 EJDG, JCW, NJM & PJL conceived and planned the experiments. EJDG, JCW, AS & AN carried out the
224 experiments. EJDG, JCW, NJM & PJL wrote the manuscript with input from all authors.

225 Experimental Procedures

226 NL4-3 molecular clones

227 pNL4-3-dE-EGFP (derived from the HIV-1 molecular clone pNL4-3 but encoding Enhanced Green
228 Fluorescent Protein (EGFP) in the *env* open reading frame (ORF), rendering Env non-functional) was
229 obtained through the AIDS Reagent Program, Division of AIDS, NIAD, NIH: Drs Haili Zhang, Yan Zhou,
230 and Robert Siliciano(44)and the complete sequence verified by Sanger sequencing. The ΔVpr mutant
231 was generated by cloning three stop codons into the Vpr open reading frame, immediately after the
232 overlap with Vif to prevent interference with that gene:
233 WT Vpr ORF sequence
234 ATGGAACAAGCCCCAGAAGACCAAGGGCCACAGAGGGAGCCATACAATGAATGGACACTAGAGCTTTTAGAGGAA
235 ΔVpr ORF sequence
236 ATGGAACAAGCCCCAGAAGACCAAGGGCCACAGAGGGAGCCATACAATGAATGGACACTAGAGCTTTAATAGTAA

237 Viral stocks

238 VSVg-pseudotyped NL4-3-dE-EGFP HIV viral stocks were generated by co-transfection with pMD.G
239 (VSVg) as previously described(5). NL4-3-dE-EGFP HIV viral stocks were titred by
240 infection/transduction of known numbers of relevant target cells under standard experimental
241 conditions followed by flow cytometry for GFP and CD4 at 48 hr to identify % infected cells.
242 Single Vpr and Vpx proteins were expressed in a modified dual promotor pHRSIN(45) vector in
243 which Vpr or Vpx expression is driven by the rous sarcoma virus (RSV) promotor, and Emerald GFP
244 expression is driven by the ubiquitin promotor. Virus was generated by co-transfection with p8.91
245 and pMD.G in 293T as previously described(5). Infectious MOI was normalised by infection in the

246 absence of reverse transcription (RTi) inhibitors, which were included where specified (see below).
247 The panel of Vpr and Vpr proteins used are detailed in **Supplementary Table 4**. Amino acid
248 sequences were codon optimized and synthesized as double stranded DNA (IDT), inserted into the
249 empty vector construct by Gibson assembly, and confirmed by sanger sequencing.

250 **CEM-T4 T-cell infections**
251 CEM-T4 T-cells were infected with concentrated NL4-3-dE-EGFP or pHRSIN lentiviral stocks by
252 spinoculation at 800 ×g for 1 h in a non-refrigerated benchtop centrifuge in complete media
253 supplemented with 10 mM HEPES. Where reverse transcription treatment was specified (RTi), cells
254 were incubated with zidovudine (10 µM) and efavirenz (100 nM) (AIDS Reagent Program, Division of
255 AIDS, NIAD, NIH) for 1 hr prior to spinoculation, and inhibitors maintained at these concentrations
256 during subsequent cell culture. For MS experiments, cells were subject to dead cell removal
257 (magnetic dead cell removal kit, Miltenyi). Subsequent sample preparation, TMT labelling, and MS
258 are described in the **supplementary methods**.

259 **Pulsed Stable isotope labelling with amino acids in cell culture (Pulsed-SILAC)**
260 For SILAC labelling, CEM-T4 T-cells were grown for at least 7 cell divisions in SILAC RPMI lacking
261 lysine and arginine (Thermo Scientific, Thermo Fisher Scientific, UK) supplemented with 10% dialysed
262 FCS (Gibco, Thermo Fisher Scientific), 100 units/ml penicillin and 0.1 mg/ml streptomycin, 280 mg/L
263 proline (Sigma, UK) and medium (K4, R6; Cambridge Isotope Laboratories, Tewksbury, MA) or heavy
264 (K8, R10; Cambridge Isotope Laboratories) $^{13}C/^{15}N$-containing lysine (K) and arginine (R) at 50 mg/L.
265 At 0 h, cells were washed in media containing only light (^{12}C /^{14}N) lysine and arginine and were
266 maintained in this media for the duration of the experiment. Additional detail on MS methods is
267 available in the **supplementary methods**

268 **Mass spectrometry Immunoprecipitation (MS-IP)**
269 CEM-T4 T-cells were lysed in 1 % NP-40. Lysates were pre-cleared with IgG-Sepharose (GE
270 Healthcare, UK) and incubated for 3 hr at 4°C with anti-HA coupled to agarose beads (Sigma EZview
271 Red Anti-HA Affinity Gel). After washing in 0.5% NP-40, samples were eluted with 0.5 mg/ml HA
272 peptide at 37°C for 1 hr. Additional detail on MS methods is available in the **supplementary**
273 **methods**. Proteins defined as co-immunoprecipitating with Vpr were detected with at least 3
274 peptides in the Vpr condition, not identified in the control condition, and were present in <20% of
275 MS-IP available in the Crapome(46) database http://crapome.org/.

276 **Antibodies**
277 Antibodies against the following proteins were used for immunoblot, by manufacturer: TASOR
278 (HPA006735) - Atlas. BBX (A303-151A), HLTF (A300-230A), RALY (A302-070A), ZNF512B (A303-234A)
279 - Bethyl. SMN1/2 (2F1) - Cell signalling. ESCO2 (NB100-87021) - Novus. UNG2 (2C12) - Origene. Vpr
280 (51143-I-AP) – Proteintech. CCNB1 (SC-245), ZGPAT (SC-51524) – Santa Cruz. β-actin (AC74) – Sigma.
281 p24 (ab9071), VCP (ab11433) – Abcam. Anti-CD4-AF647 (clone OKT4; BioLegend) and anti-CD271
282 (NGFR)-APC (clone ME20.4, Biolegend) were used for flow cytometry. The following secondary
283 antibodies were used: goat anti-mouse-HRP and anti-rabbit-HRP (immunoblot, Jackson
284 ImmunoResearch, West Grove, PA).

285 **J-LAT reactivation experiments.**
286 JLAT A1 cells were transduced with Cre recombinase, NL4-3 Vpr or HIV-2 ROD Vpx within a pHRSIN
287 IRES NGFR vector(47). 24 h after transduction, cells were treated with 2 ng/ml TNFα (PeproTech,
288 300-01A). After an additional 24 h cells were stained with anti-NGFR APC and analysed for APC and
289 GFP expression by flow cytometry. Cells were gated for NGFR+ cells to exclude non-transduced cells.
290 Flow cytometry data was acquired on a BD FACSCalibur.

291 **Statistical analysis**
292 Anova and Fisher's exact test analysis were carried out as described in figure legends using
293 Graphpad Prism (v7.04). Statistical analysis of proteomics datasets is described in detail in
294 **supplementary methods,** briefly TMT multiplexed proteomics datasets were analysed using a
295 moderated T-test analysis with Benjamini-Hochberg correction(48), carried out using R (v3.3.1)(49).
296 Significance B values for pulsed SILAC analysis were calculated using Perseus(50).

297 **Data availability**
298 In addition to **Supplementary Table 1**, which includes data from all of the proteomics experiments
299 carried out here, proteomics data have been deposited to the ProteomeXchange Consortium via the
300 PRIDE(51) partner repository with the dataset identifier PXD01029.

301 **References**

302 1. Matheson NJ, Greenwood EJ, & Lehner PJ (2016) Manipulation of immunometabolism by
303 HIV-accessories to the crime? *Curr Opin Virol* 19:65-70.
304 2. Sugden SM, Bego MG, Pham TN, & Cohen EA (2016) Remodeling of the Host Cell Plasma
305 Membrane by HIV-1 Nef and Vpu: A Strategy to Ensure Viral Fitness and Persistence. *Viruses*
306 8(3).
307 3. Simon V, Bloch N, & Landau NR (2015) Intrinsic host restrictions to HIV-1 and mechanisms of
308 viral escape. *Nat Immunol* 16(6):546-553.
309 4. Matheson NJ*, et al.* (2015) Cell Surface Proteomic Map of HIV Infection Reveals Antagonism
310 of Amino Acid Metabolism by Vpu and Nef. *Cell host & microbe* 18(4):409-423.
311 5. Greenwood EJ*, et al.* (2016) Temporal proteomic analysis of HIV infection reveals
312 remodelling of the host phosphoproteome by lentiviral Vif variants. *eLife* 5.
313 6. Lahouassa H*, et al.* (2016) HIV-1 Vpr degrades the HLTF DNA translocase in T cells and
314 macrophages. *Proceedings of the National Academy of Sciences of the United States of*
315 *America*.
316 7. Hrecka K*, et al.* (2016) HIV-1 and HIV-2 exhibit divergent interactions with HLTF and UNG2
317 DNA repair proteins. *Proceedings of the National Academy of Sciences of the United States of*
318 *America* 113(27):E3921-3930.
319 8. Maudet C*, et al.* (2013) HIV-1 Vpr induces the degradation of ZIP and sZIP, adaptors of the
320 NuRD chromatin remodeling complex, by hijacking DCAF1/VprBP. *PLoS One* 8(10):e77320.
321 9. Romani B, Shaykh Baygloo N, Aghasadeghi MR, & Allahbakhshi E (2015) HIV-1 Vpr Protein
322 Enhances Proteasomal Degradation of MCM10 DNA Replication Factor through the Cul4-
323 DDB1[VprBP] E3 Ubiquitin Ligase to Induce G2/M Cell Cycle Arrest. *J Biol Chem*
324 290(28):17380-17389.
325 10. Schrofelbauer B, Yu Q, Zeitlin SG, & Landau NR (2005) Human immunodeficiency virus type 1
326 Vpr induces the degradation of the UNG and SMUG uracil-DNA glycosylases. *J Virol*
327 79(17):10978-10987.
328 11. Lv L*, et al.* (2018) Vpr Targets TET2 for Degradation by CRL4(VprBP) E3 Ligase to Sustain IL-6
329 Expression and Enhance HIV-1 Replication. *Mol Cell* 70(5):961-970 e965.
330 12. Zhou X, DeLucia M, & Ahn J (2016) SLX4-SLX1 Protein-independent Down-regulation of
331 MUS81-EME1 Protein by HIV-1 Viral Protein R (Vpr). *J Biol Chem* 291(33):16936-16947.
332 13. Lapek JD, Jr., Lewinski MK, Wozniak JM, Guatelli J, & Gonzalez DJ (2017) Quantitative
333 Temporal Viromics of an Inducible HIV-1 Model Yields Insight to Global Host Targets and
334 Phospho-Dynamics Associated with Protein Vpr. *Mol Cell Proteomics* 16(8):1447-1461.
335 14. Goh WC*, et al.* (1998) HIV-1 Vpr increases viral expression by manipulation of the cell cycle: a
336 mechanism for selection of Vpr in vivo. *Nat Med* 4(1):65-71.
337 15. Forget J, Yao XJ, Mercier J, & Cohen EA (1998) Human immunodeficiency virus type 1 vpr
338 protein transactivation function: mechanism and identification of domains involved. *J Mol*
339 *Biol* 284(4):915-923.
340 16. Zhao LJ, Mukherjee S, & Narayan O (1994) Biochemical mechanism of HIV-I Vpr function.
341 Specific interaction with a cellular protein. *J Biol Chem* 269(22):15577-15582.
342 17. Wu Y*, et al.* (2016) The DDB1-DCAF1-Vpr-UNG2 crystal structure reveals how HIV-1 Vpr
343 steers human UNG2 toward destruction. *Nat Struct Mol Biol* 23(10):933-940.
344 18. Fregoso OI & Emerman M (2016) Activation of the DNA Damage Response Is a Conserved
345 Function of HIV-1 and HIV-2 Vpr That Is Independent of SLX4 Recruitment. *MBio* 7(5).
346 19. Laguette N*, et al.* (2014) Premature activation of the SLX4 complex by Vpr promotes G2/M
347 arrest and escape from innate immune sensing. *Cell* 156(1-2):134-145.
348 20. Fischer M, Grossmann P, Padi M, & DeCaprio JA (2016) Integration of TP53, DREAM, MMB-
349 FOXM1 and RB-E2F target gene analyses identifies cell cycle gene regulatory networks.
350 *Nucleic Acids Res* 44(13):6070-6086.

351 21. Ly T, Endo A, & Lamond AI (2015) Proteomic analysis of the response to cell cycle arrests in
352 human myeloid leukemia cells. *eLife* 4.
353 22. Zhou Y & Ratner L (2000) Phosphorylation of human immunodeficiency virus type 1 Vpr
354 regulates cell cycle arrest. *Journal of virology* 74(14):6520-6527.
355 23. Jager S*, et al.* (2011) Global landscape of HIV-human protein complexes. *Nature*
356 481(7381):365-370.
357 24. Luo Y*, et al.* (2016) HIV-host interactome revealed directly from infected cells. *Nat Microbiol*
358 1(7):16068.
359 25. Boisvert FM*, et al.* (2012) A quantitative spatial proteomics analysis of proteome turnover in
360 human cells. *Mol Cell Proteomics* 11(3):M111 011429.
361 26. Tchasovnikarova IA*, et al.* (2015) GENE SILENCING. Epigenetic silencing by the HUSH complex
362 mediates position-effect variegation in human cells. *Science* 348(6242):1481-1485.
363 27. Hrecka K*, et al.* (2011) Vpx relieves inhibition of HIV-1 infection of macrophages mediated by
364 the SAMHD1 protein. *Nature* 474(7353):658-661.
365 28. Lim ES*, et al.* (2012) The ability of primate lentiviruses to degrade the monocyte restriction
366 factor SAMHD1 preceded the birth of the viral accessory protein Vpx. *Cell host & microbe*
367 11(2):194-204.
368 29. Yurkovetskiy L*, et al.* (2018) Primate immunodeficiency virus Vpx and Vpr counteract
369 transcriptional repression of proviruses by the HUSH complex. *bioRxiv*.
370 30. Chougui G*, et al.* (2018) HIV-2/SIV viral protein X counteracts HUSH repressor complex. *Nat*
371 *Microbiol*.
372 31. Ersing I*, et al.* (2017) A Temporal Proteomic Map of Epstein-Barr Virus Lytic Replication in B
373 Cells. *Cell Rep* 19(7):1479-1493.
374 32. Weekes MP*, et al.* (2014) Quantitative temporal viromics: an approach to investigate host-
375 pathogen interaction. *Cell* 157(6):1460-1472.
376 33. Diamond DL*, et al.* (2010) Temporal proteome and lipidome profiles reveal hepatitis C virus-
377 associated reprogramming of hepatocellular metabolism and bioenergetics. *PLoS Pathog*
378 6(1):e1000719.
379 34. Guenzel CA, Herate C, & Benichou S (2014) HIV-1 Vpr-a still "enigmatic multitasker". *Front*
380 *Microbiol* 5:127.
381 35. Gummuluru S & Emerman M (1999) Cell cycle- and Vpr-mediated regulation of human
382 immunodeficiency virus type 1 expression in primary and transformed T-cell lines. *Journal of*
383 *virology* 73(7):5422-5430.
384 36. Bolton DL & Lenardo MJ (2007) Vpr cytopathicity independent of G2/M cell cycle arrest in
385 human immunodeficiency virus type 1-infected CD4+ T cells. *Journal of virology* 81(17):8878-
386 8890.
387 37. Hohne K*, et al.* (2016) Virion encapsidated HIV-1 Vpr induces NFAT to prime non-activated T
388 cells for productive infection. *Open Biol* 6(7).
389 38. Liang Z*, et al.* (2015) HIV-1 Vpr protein activates the NF-kappaB pathway to promote G2/M
390 cell cycle arrest. *Virol Sin* 30(6):441-448.
391 39. Liu R*, et al.* (2014) HIV-1 Vpr stimulates NF-kappaB and AP-1 signaling by activating TAK1.
392 *Retrovirology* 11:45.
393 40. Muthumani K*, et al.* (2006) The HIV-1 Vpr and glucocorticoid receptor complex is a gain-of-
394 function interaction that prevents the nuclear localization of PARP-1. *Nat Cell Biol* 8(2):170-
395 179.
396 41. Shimura M*, et al.* (2011) Epigenetic displacement of HP1 from heterochromatin by HIV-1 Vpr
397 causes premature sister chromatid separation. *J Cell Biol* 194(5):721-735.
398 42. Vassena L, Giuliani E, Matusali G, Cohen EA, & Doria M (2013) The human immunodeficiency
399 virus type 1 Vpr protein upregulates PVR via activation of the ATR-mediated DNA damage
400 response pathway. *J Gen Virol* 94(Pt 12):2664-2669.

401 43. Richard J, Sindhu S, Pham TN, Belzile JP, & Cohen EA (2010) HIV-1 Vpr up-regulates
402 expression of ligands for the activating NKG2D receptor and promotes NK cell-mediated
403 killing. *Blood* 115(7):1354-1363.
404 44. Zhang H*, et al.* (2004) Novel single-cell-level phenotypic assay for residual drug susceptibility
405 and reduced replication capacity of drug-resistant human immunodeficiency virus type 1.
406 *Journal of virology* 78(4):1718-1729.
407 45. van den Boomen DJ*, et al.* (2014) TMEM129 is a Derlin-1 associated ERAD E3 ligase essential
408 for virus-induced degradation of MHC-I. *Proceedings of the National Academy of Sciences of*
409 *the United States of America* 111(31):11425-11430.
410 46. Mellacheruvu D*, et al.* (2013) The CRAPome: a contaminant repository for affinity
411 purification-mass spectrometry data. *Nat Methods* 10(8):730-736.
412 47. Matheson NJ, Peden AA, & Lehner PJ (2014) Antibody-free magnetic cell sorting of
413 genetically modified primary human CD4+ T cells by one-step streptavidin affinity
414 purification. *PLoS One* 9(10):e111437.
415 48. Schwammle V, Leon IR, & Jensen ON (2013) Assessment and improvement of statistical tools
416 for comparative proteomics analysis of sparse data sets with few experimental replicates.
417 *Journal of proteome research* 12(9):3874-3883.
418 49. R Core Team (2013) R: A language and environment for statistical computing. *Vienna,*
419 *Austria. http://www.R-project.org/.*
420 50. Tyanova S*, et al.* (2016) The Perseus computational platform for comprehensive analysis of
421 (prote)omics data. *Nat Methods* 13(9):731-740.
422 51. Vizcaino JA*, et al.* (2016) 2016 update of the PRIDE database and its related tools. *Nucleic*
423 *acids research* 44(22):11033.

424 **Figure legends**

425 **Fig. 1. Proteomic analysis of the effect of Vpr in HIV infection. a**, Graphical summary of the HIV and
426 ΔVpr HIV infection TMT experiment. **b,** FACS plots showing the quantification of infection in an
427 example replicate for each of the three conditions. **c,** Scatterplots displaying pairwise comparisons
428 between WT, ΔVpr and mock-infected cells. Each point represents a single protein, with HIV proteins
429 and host proteins of interest highlighted with different symbols (see key). **d,** Principle component
430 analysis of the samples in this experiment.

431 **Fig. 2. Analysis of the nature of Vpr mediated proteome remodelling.**

432 **a**, Graphical summary of the Vpr viral particle TMT experiment. **b,** Scatterplot displaying pairwise
433 comparison between cells exposed to empty or Vpr bearing viral particles. **c**, Scatterplot comparing
434 pairwise comparisons from two proteomics experiments, demonstrating the effect of Vpr in the
435 context of HIV-1 infection (x axis, as shown in **Fig. 1a**) or through cellular exposure to Vpr protein
436 alone (y axis, as shown in **Fig. 2a**). **d**, scatterplots showing the pairwise comparison between each
437 Vpr mutant tested and empty vector control, with defined groups of 302 Vpr depleted and 413
438 increased proteins highlighted in blue and red respectively. **e**, Heatmap showing the behaviour of
439 the 100 proteins most depleted by Vpr particles (blue) and increased (red) within the defined highly
440 modulated subsets. Colour indicates the $\log_2$ fold change of each protein in each condition
441 compared to empty particle treatment. **f,** Graphical summary of the DCAF1 KD experiment. **g,**
442 Scatterplots showing the pairwise comparison between the 6 or 24 h timepoint with the 0 h
443 condition for each sh-transduced cell line.

444 **Fig. 3. Identifying direct targets for Vpr mediated decay.**

445 **a,** Graphical summary of the pulsed SILAC experiment. **b,** Scatterplots showing the changes to
446 protein stability of proteins after 6 or 24 hours of exposure to Vpr bearing lentivirus compared to
447 control lentivirus, with defined groups of 302 Vpr depleted (blue) and 413 increased (red) proteins
448 highlighted. **c,** Expanded view of proteins degraded within 6 hours of Vpr exposure. Significantly
449 degraded (Sig.B<0.01) proteins are highlighted in gold. Previously described Vpr targets HLTF,
450 MUS81 and ZGPAT are shown in purple. **d**, Graphical summary of the direct targets for Vpr mediated
451 degradation. Proteins highlighted in purple are previously described Vpr targets, proteins with red
452 text were predicted as potential Vpr targets based on their temporal profile of depletion in
453 Greenwood & Matheson, 2016(5).

454 **Fig. 4. Identification of proteome changes conserved between human and primate lentiviral Vpr**
455 **lineages. a**, Graphical summary of the TMT experiment testing conservation of Vpr functions. **b**,
456 Scatterplots showing the pairwise comparison between each Vpr tested and empty vector control
457 with defined groups of 302 Vpr depleted (blue) and 413 increased (red) proteins highlighted. **c,**
458 Heatmap showing the behaviour of the 100 proteins most depleted by Vpr particles (blue) and
459 increased (red) within the defined highly modulated subsets. Colour indicates the $\log_2$ fold change of
460 each protein in each condition compared to empty vector virus transduction. **d,** Bar chart showing
461 the significantly Vpr depleted group showing profound (more than 50%) depletion in more than one
462 lineage, of the four lineages tested (HIV-1/SIVcpz, HIV-2/SIVsmm, SIVagm, SIVrcm). Gold bars
463 indicate proteins identified as direct targets for Vpr mediated degradation, DCAF1, known to interact
464 with multiple lineages, is highlight in purple. **e**, Immunoblot of example known, non-conserved and
465 conserved targets of Vpr mediated depletion. N.B. The HIV-2 Vpr is a primary isolate HIV-2 Vpr
466 (7312a), while the proteomics experiment included HIV-2 ROD Vpr. **f,** Scatterplots showing the
467 pairwise comparison between each Vpr tested and empty vector control with HuSH complex
468 components highlighted. **g**, Bar graph of GFP percentage positive of JLAT-A1 cells after transduction
469 with control (Cre recombinase), Vpr or Vpx proteins and treatment with TNFα. Mean and SEM of
470 three biological replicates per condition are shown. p-values determined by ordinary one-way
471 ANOVA with Bonferroni comparison between Vpr/Vpx treatment and control treated cells. **h,**
472 Immunoblot of TASOR in cells transduced with a panel of Vpx and Vpr proteins.

Figure 1

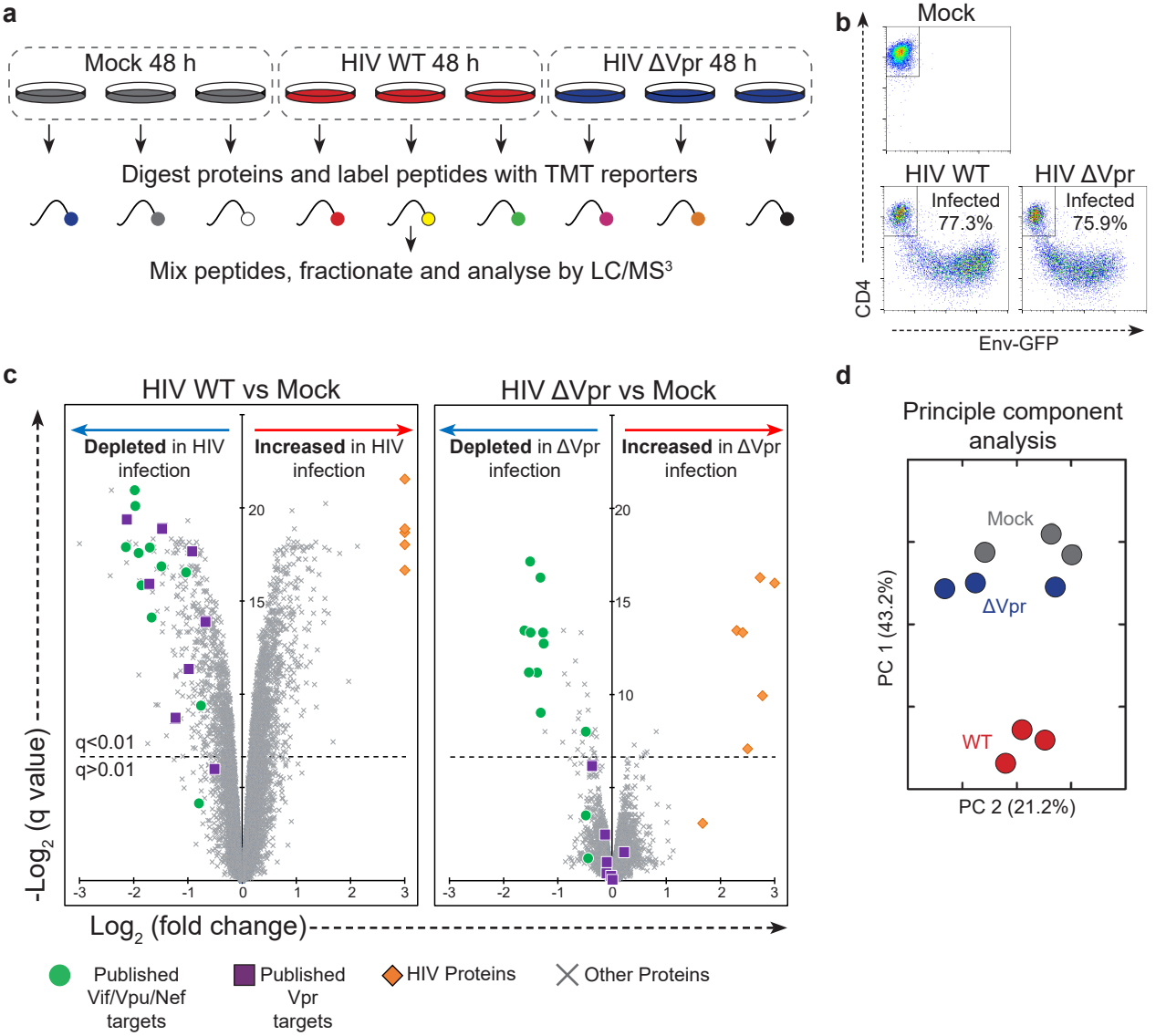
a
Mock 48 h
HIV WT 48 h
HIV ΔVpr 48 h
Digest proteins and label peptides with TMT reporters
Mix peptides, fractionate and analyse by LC/MS3
b
Mock
HIV WT
HIV ΔVpr
Infected 77.3%
Infected 75.9%
CD4
Env-GFP
c
HIV WT vs Mock
HIV ΔVpr vs Mock
Depleted in HIV infection
Increased in HIV infection
Depleted in ΔVpr infection
Increased in ΔVpr infection
q<0.01
q>0.01
-Log2 (q value)
Log2 (fold change)
Published Vif/Vpu/Nef targets
Published Vpr targets
HIV Proteins
Other Proteins
d
Principle component analysis
Mock
ΔVpr
WT
PC 1 (43.2%)
PC 2 (21.2%)

Figure 2

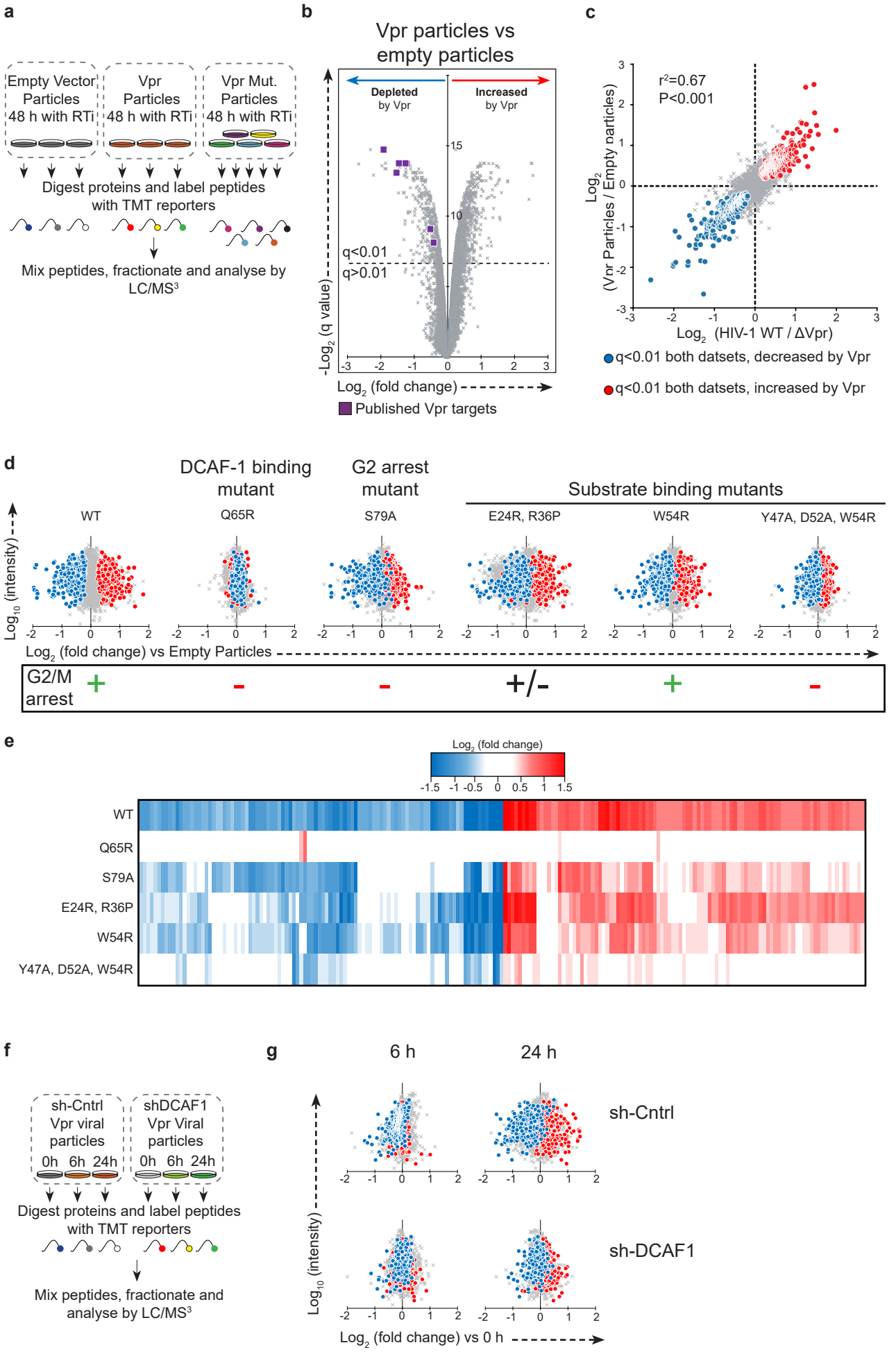
a
Empty Vector Particles 48 h with RTi
Vpr Particles 48 h with RTi
Vpr Mut. Particles 48 h with RTi
Digest proteins and label peptides with TMT reporters
Mix peptides, fractionate and analyse by LC/MS3
b
Vpr particles vs empty particles
Depleted by Vpr
Increased by Vpr
q<0.01
q>0.01
-Log2 (q value)
Log2 (fold change)
Published Vpr targets
c
r2=0.67
P<0.001
Log2 (Vpr Particles / Empty particles)
Log2 (HIV-1 WT / ΔVpr)
q<0.01 both datsets, decreased by Vpr
q<0.01 both datsets, increased by Vpr
d
DCAF-1 binding mutant
G2 arrest mutant
Substrate binding mutants
WT
Q65R
S79A
E24R, R36P
W54R
Y47A, D52A, W54R
Log10 (intensity)
Log2 (fold change) vs Empty Particles
G2/M arrest
+
-
-
+/-
+
-
e
Log2 (fold change)
WT
Q65R
S79A
E24R, R36P
W54R
Y47A, D52A, W54R
f
sh-Cntrl Vpr viral particles
shDCAF1 Vpr Viral particles
0h 6h 24h
Digest proteins and label peptides with TMT reporters
Mix peptides, fractionate and analyse by LC/MS3
g
6 h
24 h
sh-Cntrl
sh-DCAF1
Log10 (intensity)
Log2 (fold change) vs 0 h

Figure 3

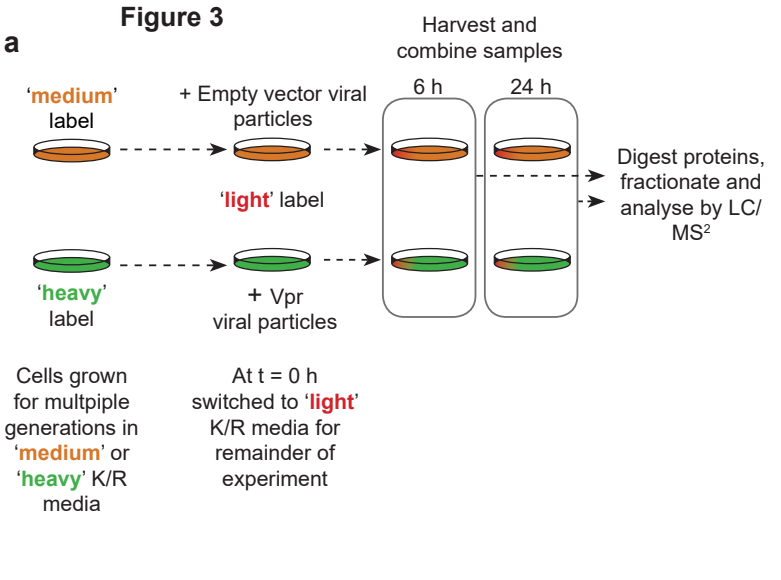

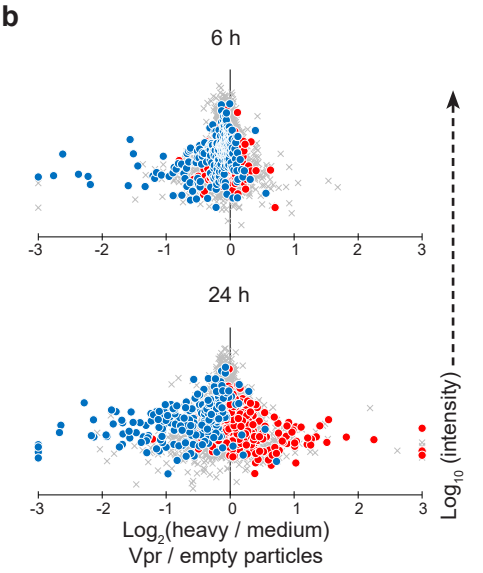

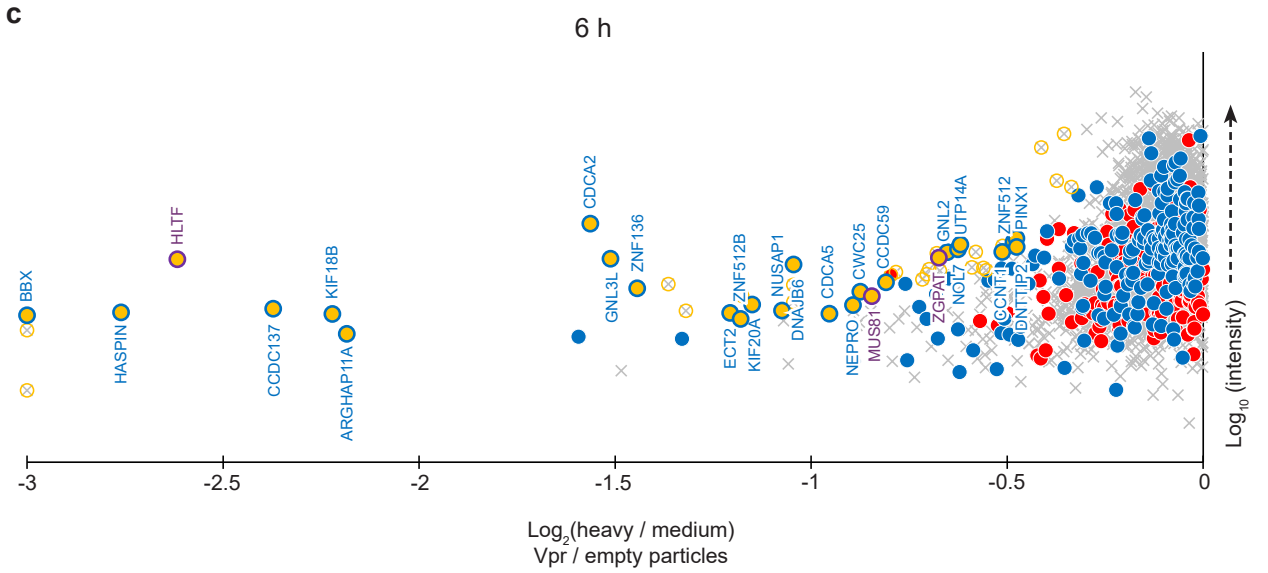

d

Accession	Gene	Vpr necessary	Incoming Vpr sufficient	Degraded within 6 h	Co-IP
Q56NI9	ESCO2	Yes	Yes	ND	Yes
Q16637	SMN1 / SMN2	Yes	Yes	NS	Yes
Q14527	HLTF	Yes	Yes	Yes	-
Q96KM6	ZNF512B	Yes	Yes	Yes	-
Q8WY36	BBX	Yes	Yes	Yes	Yes
A6NFI3	ZNF316	Yes	Yes	Yes	-
Q8NI77	KIF18A	Yes	Yes	ND	Yes
Q8TF76	HASPIN	Yes	Yes	Yes	-
Q9Y4B6	VPRBP	Yes	Yes	NS	Yes
Q96FF9	CDCA5	Yes	Yes	Yes	-
Q6PK04	CCDC137	Yes	Yes	Yes	-
Q9NXE8	CWC25	Yes	Yes	Yes	-
Q86Y91	KIF18B	Yes	Yes	Yes	-
Q6P4F7	ARHGAP11A	Yes	Yes	Yes	-
Q6NW34	NEPRO	Yes	Yes	Yes	-
Q9BVJ6	UTP14A	Yes	Yes	Yes	-
Q9NVN8	GNL3L	Yes	Yes	Yes	-
Q5QJE6	DNTTIP2	Yes	Yes	Yes	-
Q69YH5	CDCA2	Yes	Yes	Yes	-

Accession	Gene	Vpr necessary	Incoming Vpr sufficient	Degraded within 6 h	Co-IP
Q96BK5	PINX1	Yes	Yes	Yes	-
Q8N5A5	ZGPAT	Yes	Yes	Yes	-
Q13823	GNL2	Yes	Yes	Yes	-
Q9UHI6	DDX20	Yes	Yes	NS	Yes
Q96ME7	ZNF512	Yes	Yes	Yes	-
Q14586	ZNF267	Yes	Yes	NS	Yes
Q9H8V3	ECT2	Yes	Yes	Yes	-
P57678	GEMIN4	Yes	Yes	NS	Yes
P52701	MSH6	Yes	Yes	NS	Yes
O75190	DNAJB6	Yes	Yes	Yes	-
Q96NY9	MUS81	Yes	Yes	Yes	-
O60563	CCNT1	Yes	Yes	Yes	-
Q9P031	CCDC59	Yes	Yes	Yes	-
Q9UIS9	MBD1	Yes	Yes	NS	Yes
Q9UMY1	NOL7	Yes	Yes	Yes	-
Q6ZN55	ZNF574	Yes	Yes	NS	Yes
Q9BXS6	NUSAP1	Yes	Yes	Yes	-
O95235	KIF20A	Yes	Yes	Yes	-
P35251	RFC1	Yes	Yes	NS	Yes

ND: Not detected in this experiment
NS: Degraded with Sig.B >0.01

Figure 4

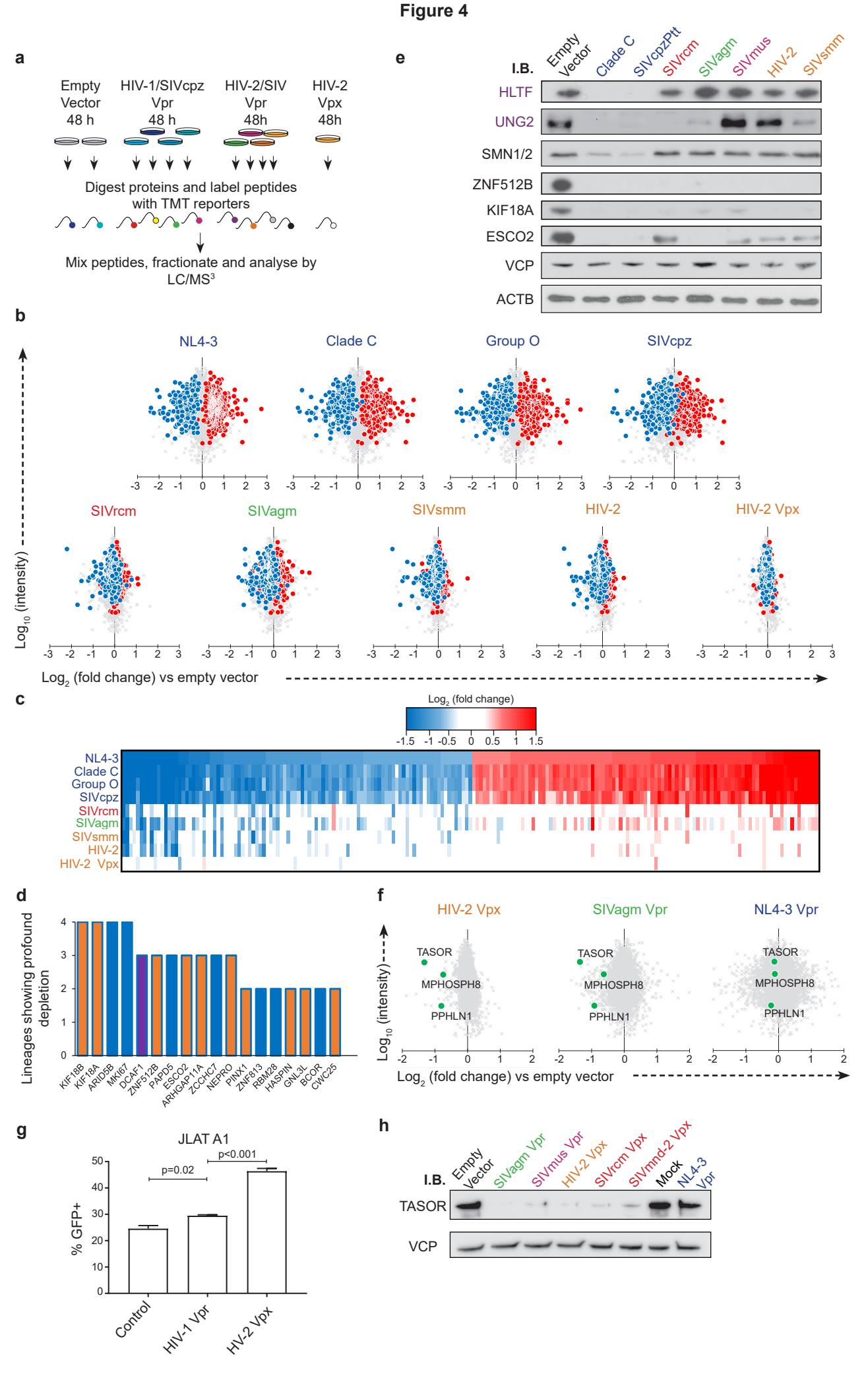
a
Empty Vector 48 h
HIV-1/SIVcpz Vpr 48 h
HIV-2/SIV Vpr 48h
HIV-2 Vpx 48h
Digest proteins and label peptides with TMT reporters
Mix peptides, fractionate and analyse by LC/MS3
e
I.B.
Empty Vector
Clade C
SIVcpzPtt
SIVrcm
SIVagm
SIVmus
HIV-2
SIVsmm
HLTF
UNG2
SMN1/2
ZNF512B
KIF18A
ESCO2
VCP
ACTB
b
NL4-3
Clade C
Group O
SIVcpz
SIVrcm
SIVagm
SIVsmm
HIV-2
HIV-2 Vpx
Log10 (intensity)
Log2 (fold change) vs empty vector
c
Log2 (fold change)
-1.5 -1 -0.5 0 0.5 1 1.5
NL4-3
Clade C
Group O
SIVcpz
SIVrcm
SIVagm
SIVsmm
HIV-2
HIV-2 Vpx
d
Lineages showing profound depletion
KIF18B
KIF18A
ARID5B
MKI67
DCAF1
ZNF512B
PAPD5
ESCO2
ARHGAP11A
ZCCHC7
NEPRO
PINX1
ZNF813
RBM28
HASPIN
GNL3L
BCOR
CWC25
f
HIV-2 Vpx
SIVagm Vpr
NL4-3 Vpr
TASOR
MPHOSPH8
PPHLN1
Log10 (intensity)
Log2 (fold change) vs empty vector
g
JLAT A1
p=0.02
p<0.001
% GFP+
Control
HIV-1 Vpr
HIV-2 Vpx
h
I.B.
Empty Vector
SIVagm Vpr
SIVmus Vpr
HIV-2 Vpx
SIVrcm Vpx
SIVmnd-2 Vpx
Mock
NL4-3 Vpr
TASOR
VCP

473 **Supplementary Figure & Table legends**

474 **Supplementary Fig. 1. Example proteins modulated by Vpr**

475 **a,** Scatterplots displaying pairwise comparisons between WT, ΔVpr and mock-infected cells. Vpr
476 depleted proteins identified in this work are highlighted in blue, UNG, ZGPAT and HLTF are
477 previously identified targets for Vpr mediated degradation, shown in purple, while CCNB1 is
478 increased by Vpr (red). **b,** Scatterplot displaying pairwise comparison between cells exposed to
479 empty or Vpr bearing viral particles. **c,** Scatterplot comparing pairwise comparisons from two
480 proteomics experiments, demonstrating the effect of Vpr in the context of HIV-1 infection (as shown
481 in **Fig.1a**, x-axis) or through cellular exposure to Vpr protein alone (**Fig. 2a**, y-axis). **d,** Bar charts
482 showing the Vpr mediated changes in protein abundance in both proteomics experiments of the
483 proteins highlighted in this figure. **e,** Immunoblot of proteins highlighted in this figure.

484 **Supplementary Fig. 2. Effect of DCAF1 Knockdown on Vpr modulated proteins.**

485 Scatterplots displaying pairwise comparison between Sh-Control and Sh-DCAF1 cells, with defined
486 groups of 302 Vpr depleted (blue) and 413 increased (red) proteins highlighted. DCAF1 is highlighted
487 in purple.

488 **Supplementary Fig. 3. Additional details of the Vpr WT and Mutant experiment in Fig. 2.**

489 **a,** Immunoblot of purified virus preparations used to infect cells for the proteomics experiment
490 displayed in **Fig 2a**. **b,** Bar chart showing the average scaled abundance of matrix, capsid and
491 integrase peptides detected in the cell lysate by MS. Bars show mean and standard deviation. **c,** 7-
492 AAD stain of cells exposed to empty vector, or Vpr wild type or Vpr mutants. Gate shows the
493 percentage of cells with 4n DNA content.

494 **Supplementary Fig. 4. Cell cycle regulation of Vpr modulated proteins.**

495 **a,** Ly, 2015 contains a proteomic analysis of NB4 cells treated with RO-3306 cells arrested in G2/M
496 with the PLK1 inhibtor RO-3306. Scatterplot showing the pairwise comparison of abundance of
497 proteins isolated from RO-3306 treated vs mock treated cells. Groups of proteins defined in the
498 current study of 302 Vpr depleted (blue) and 413 increased (red) proteins are highlighted, indicating
499 the behaviour of these proteins in NB4 cells arrested at G2/M.

500 **b,** Correlation of the Vpr mediated change in cyclin abundance in the present study (x-axis), with RO-
501 3306 mediated changes in NB4 cells in Ly, 2015. Changes in cyclin abundance in HIV infection are
502 assumed to be secondary to cell cycle arrest, and thus this correlation indicates the concordance
503 between effects secondary to cell cycle arrest between the two datasets.

504 **c,** Pie charts showing the overlap between changes in the present study and changes induced by
505 G2/M arrest in Ly, 2015. Left panel shows the behaviour of all proteins quantified in both the
506 present study (**Fig.1a** and **Fig.2a**) and Ly, 2015, i.e. a total of 1643 proteins were quantified in both
507 datasets, of which 1100 proteins did not significantly change in G2/M arrest, 260 proteins were
508 significantly depleted in G2/M arrested cells, and 283 proteins were significantly increased in G2/M
509 arrested cells. Middle panel shows the behaviour the defined group of 302 Vpr depleted proteins.
510 I.e. of 302 proteins, a total of 90 proteins were detected in Ly, 2015, 58 of which did not significantly
511 change in G2/M arrest, 18 were significantly depleted in G2/M arrest and 14 were significantly
512 increased in G2/M arrest. † Indicates the fraction in each case where the change induced by cell

513 cycle arrest is in the same direction as the effect of Vpr, i.e. the fraction for which cell cycle arrest
514 could explain the Vpr mediated protein changes. Right panel shows the behaviour of the defined
515 group of 413 Vpr increased proteins.

516 **d,** Fischer, 2016, define lists of 115 proteins whose expression peaks in G1/S phase and 174 proteins
517 whose expression peaks in G2/M phase. Pie-charts show the overlap between these lists and (left)
518 all proteins detected in the present study, (middle) proteins defined as being depleted by Vpr, and
519 (right) proteins defined as being increased by Vpr. As in the proteomics dataset, there is some
520 enrichment of proteins with peak expression in G2/M within Vpr increased proteins, and some
521 enrichment of proteins with peak expression in G1/S in Vpr depleted proteins, consistent with some
522 effects being secondary to cell cycle arrest, but these effects are in the minority.

523 **Supplementary Fig. 5. Vpr mediated depletion of proteins predicted to be Vpr targets based on**
524 **their temporal profile in HIV-1 infection.**

525 Scatterplots displaying pairwise comparisons between WT, ΔVpr and mock-infected cells (left and
526 middle, as in **Fig.1c**) or between Vpr viral particle and empty viral particle treated cells (right, as in
527 **Fig.2b**). Highlighted are a group of 13 proteins were identified in Greenwood & Matheson, 2015(5),
528 as having a highly similar temporal profile of HIV mediated depletion as that of known Vpr targets
529 UNG and HLTF.

530 **Supplementary Fig. 6. Gene ontology enrichment within Vpr modulated proteins.**

531 **a,** All significant (FDR q<0.05) enriched gene ontology molecular function terms with (left) Vpr
532 depleted and (right) Vpr increased proteins. Minimally redundant terms of interest are highlighted in
533 bold. **b,** All Significant (FDR q<0.05) enriched gene ontology cellular compartment terms with (top)
534 Vpr depleted and (bottom) Vpr increased proteins.

535 **Supplementary Fig. 7. MS-IP approach to identify direct targets for Vpr mediated degradation.**

536 **a,** Graphical summary of the MS-IP experiment. MLN4924 is a pan-Cullin inhibitor. **b,** 20 most
537 abundant proteins identified by Co-IP determined by unique peptides. Proteins falling within the
538 defined list of 302 Vpr depleted and 413 Vpr increased proteins are highlighted in blue and red
539 respectively. Cul4A, which is neither depleted or increased, but is predicted to co-IP with Vpr, is
540 shown in black. **c,** The same 20 proteins with signal intensity rather than peptide number shown. **d,**
541 Pie chart indicating the overlap between the proteins co-immunoprecipitated with Vpr and the
542 defined list of 302 Vpr decreased (blue) and 413 Vpr increased proteins (red), and proteins detected
543 but falling into neither list (grey). **e**, Bar chart showing the enrichment of Vpr depleted and Vpr
544 increased proteins within proteins co-immunoprecipitated with Vpr compared to the expected
545 numbers of proteins that would be co-immunopreciptated from each group by chance. p-value
546 indicates a Fisher's exact test of a 2x2 contingency table (Vpr depleted/increased, identified by co-
547 IP/not identified), indicating that the two criteria are significantly linked.

548 **Supplementary Fig. 8. Additional information relating to expanded panel of primate lentiviral Vpr**
549 **and Vpx varients.**

550 **a,** Phylogenetic tree of primate lentiviruses based on an alignment of Vif nucleic acid sequences,
551 with 5 major lineages of primate lentiviruses labelled. Information on Vpr and Vpx activity based on
552 a selected number of isolates tested in each lineage in Lim, 2012(28) **b** 7-AAD stain of cells
553 transduced with empty vector or Vpr/Vpx proteins. Gate shows the percentage of cells with 4n DNA
554 content. **c,** Scatterplots displaying pairwise comparisons between Vpr/Vpx transduced cells and

555 empty vector. Labelled proteins are direct targets for Vpr mediated degradation that are depleted by
556 Vpr varients from at least 3 different lineages.

557 **Supplementary table 1. Interactive database of protein changes in the datasets presented here.**

558 **Supplementary table 2. Behaviour of previously described Vpr targets in these datasets**

559 **Supplementary table 3. Connections between Vpr depleted proteins and known Vpr phenotypes**
560 Underlined proteins have been identified here as direct targets for Vpr mediated depletion.

561 **Supplementary table 4. Vpr and Vpx variants tested.**

Supplementary Fig.1

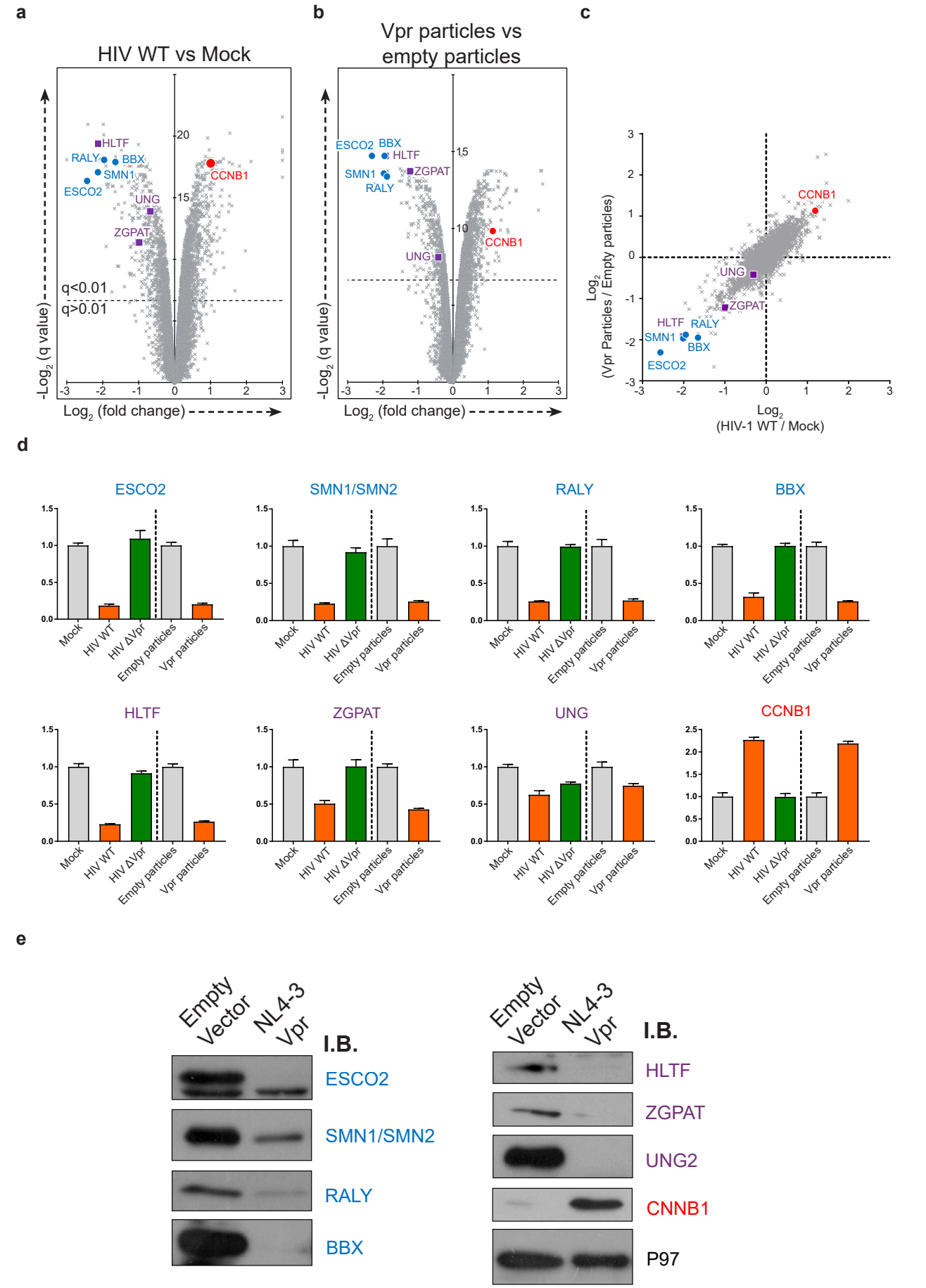

Supplementary Fig.2

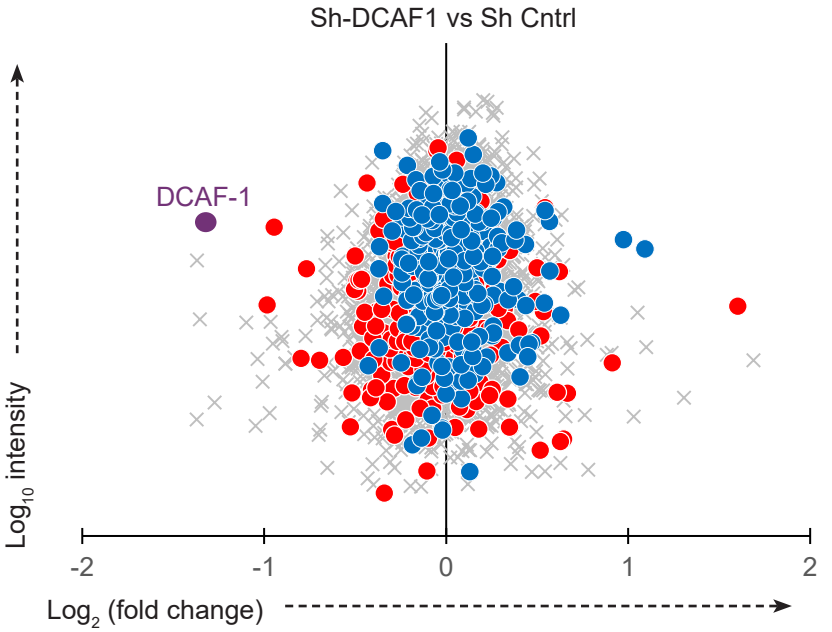

Supplementary Fig.3

a

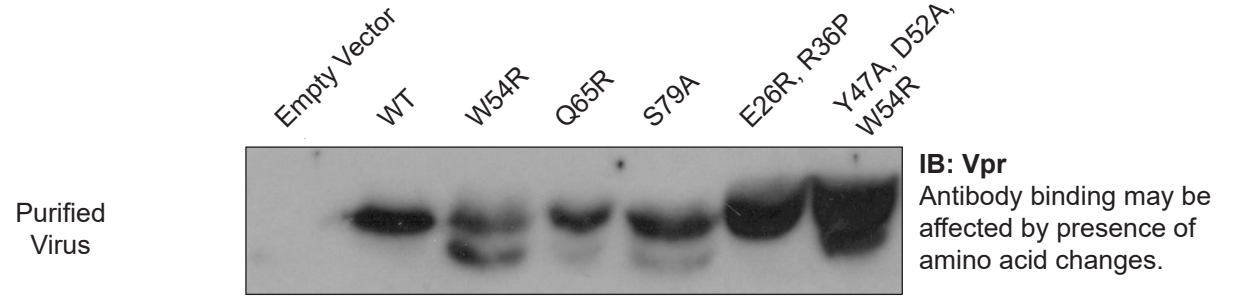

b

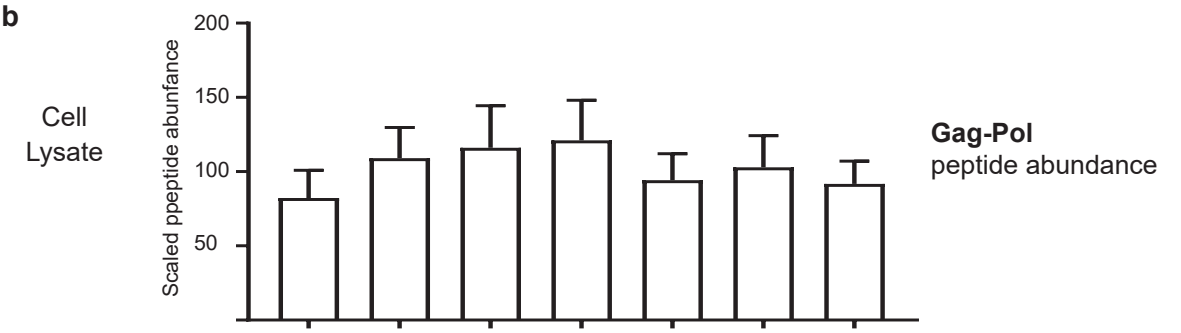

c

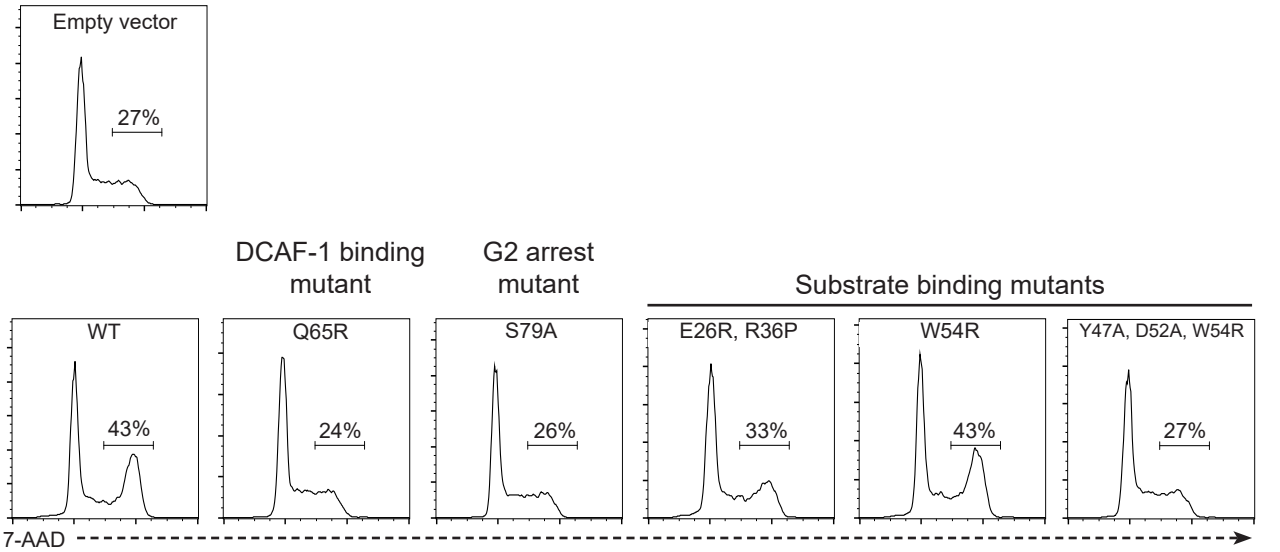

Supplementary Fig. 6

a

GO: Molecular Function

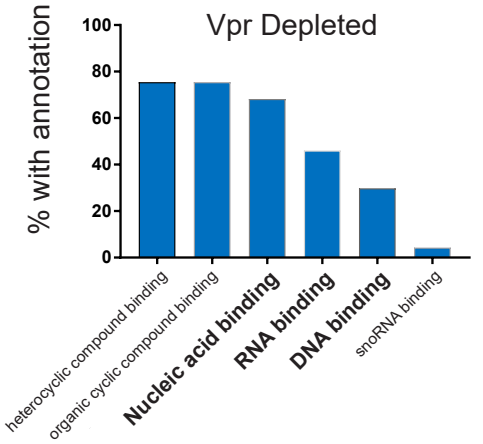

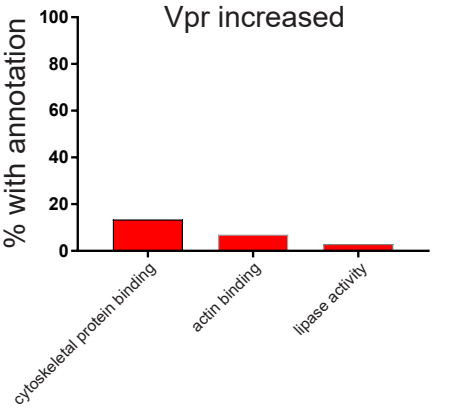

b

GO:Cellular Compartment

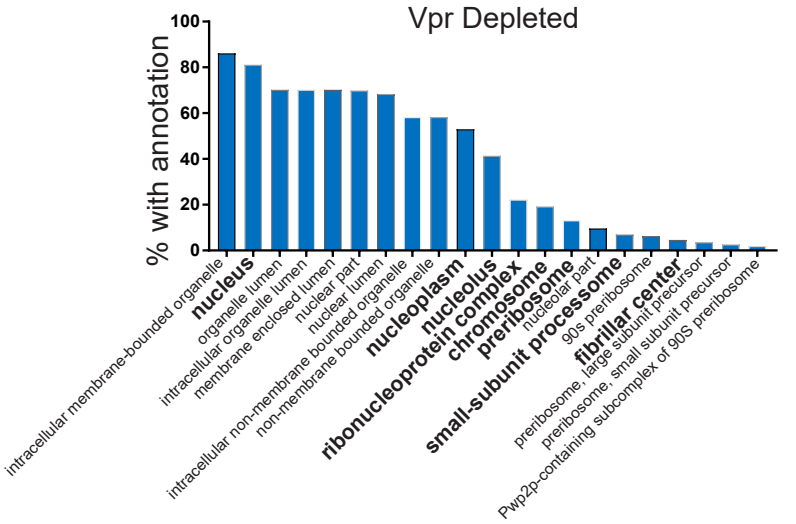

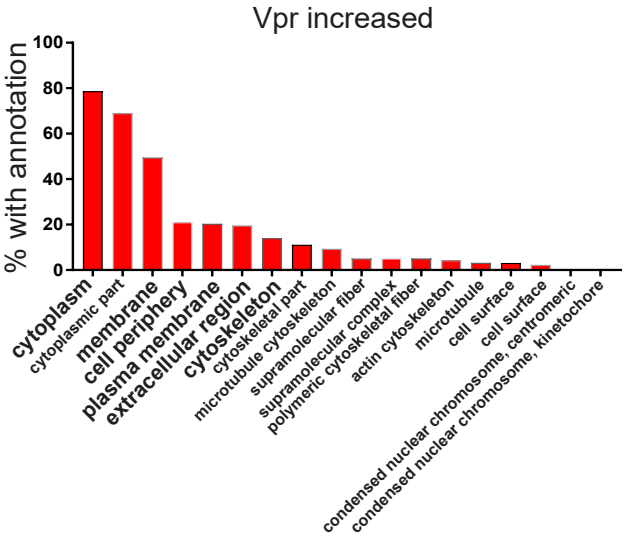

Supplementary Fig. 5

a

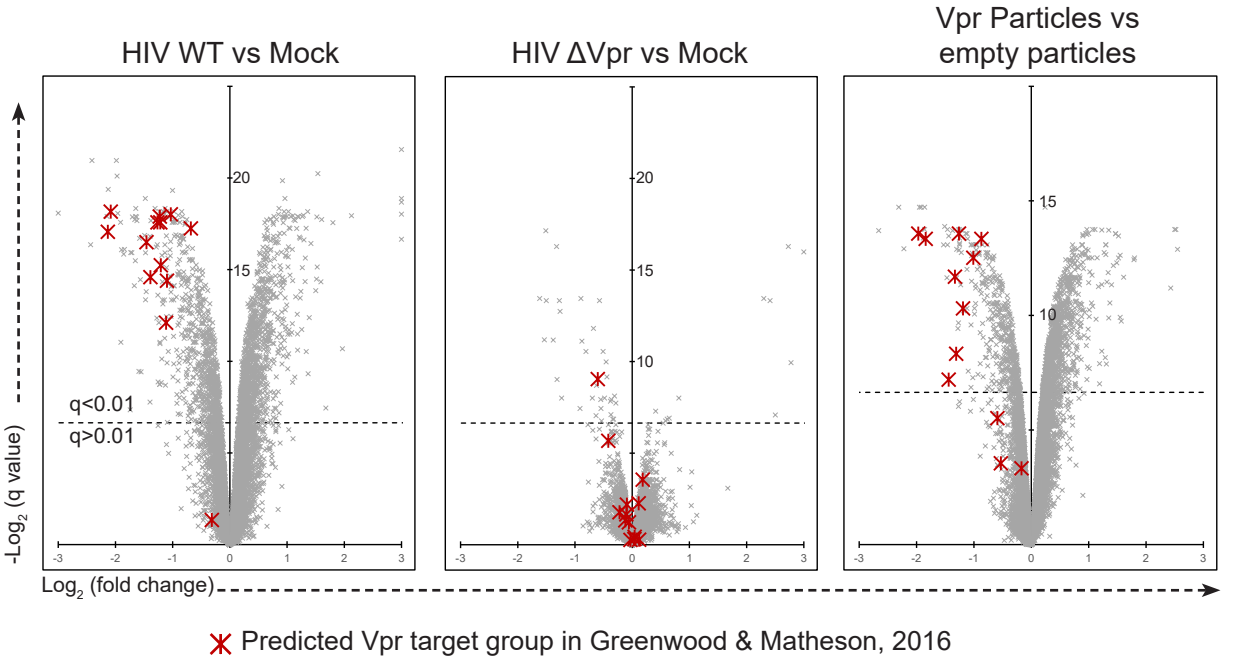

Supplementary Fig. 4

a Ly, 2015, Proteomics in G2/M arrested cells using PLK1 inhibitor RO-3306

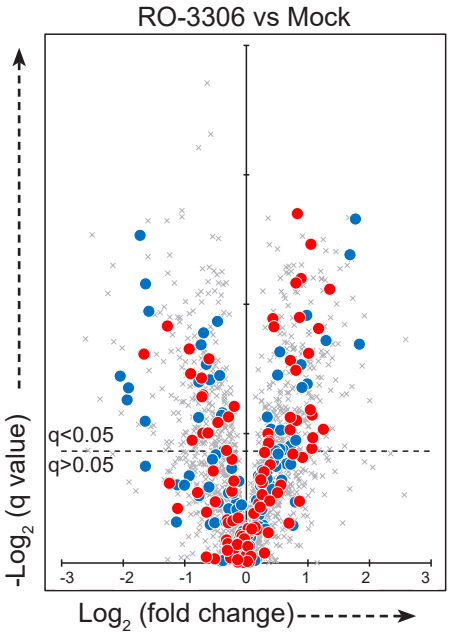

b

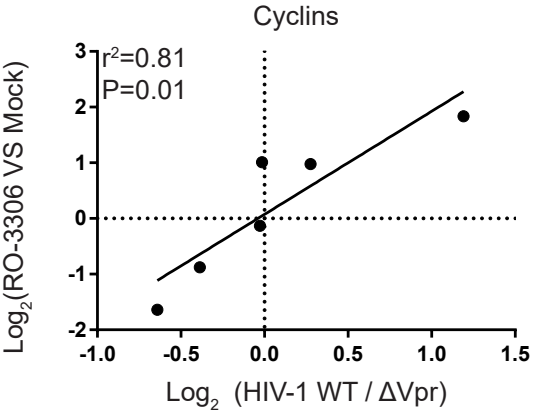

c

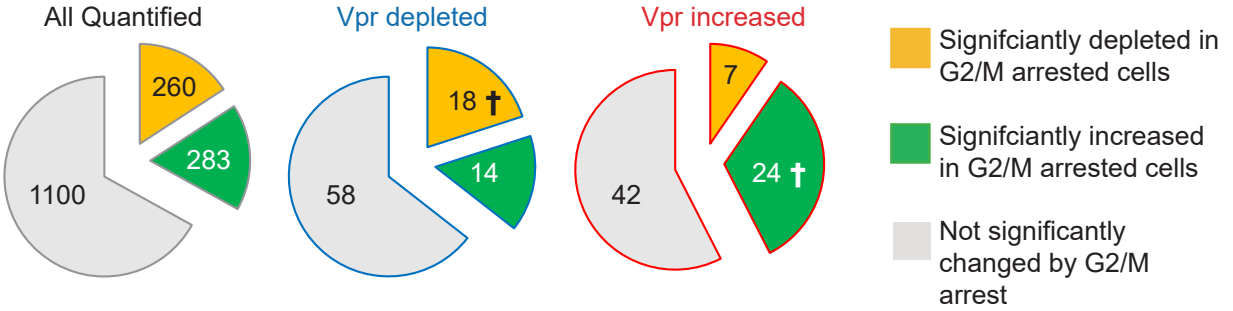

d Fischer, 2016 - Transcriptional anlalysis

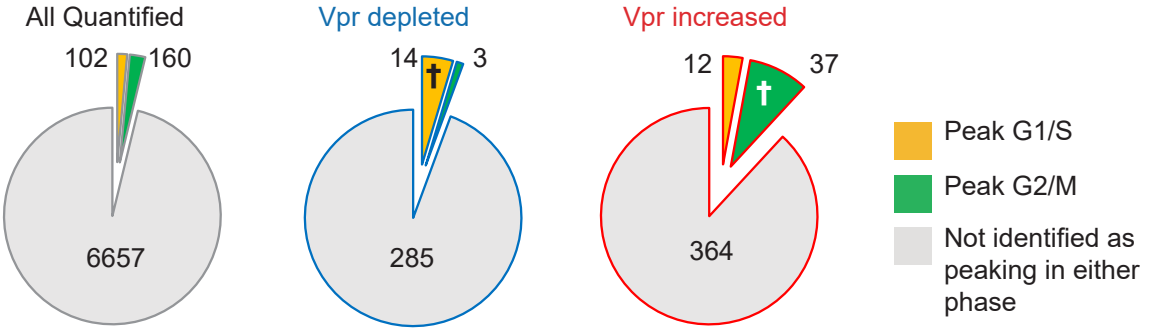

Supplementary Fig.7

a

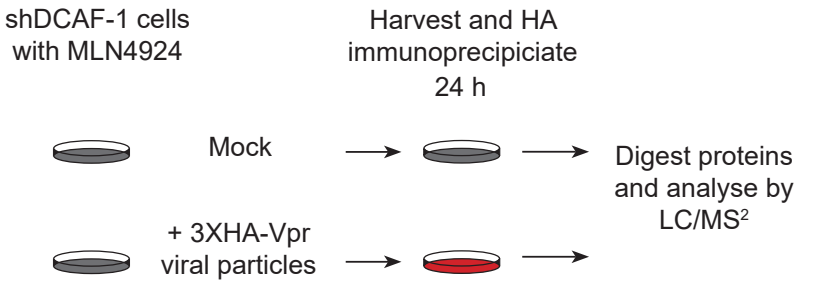

b

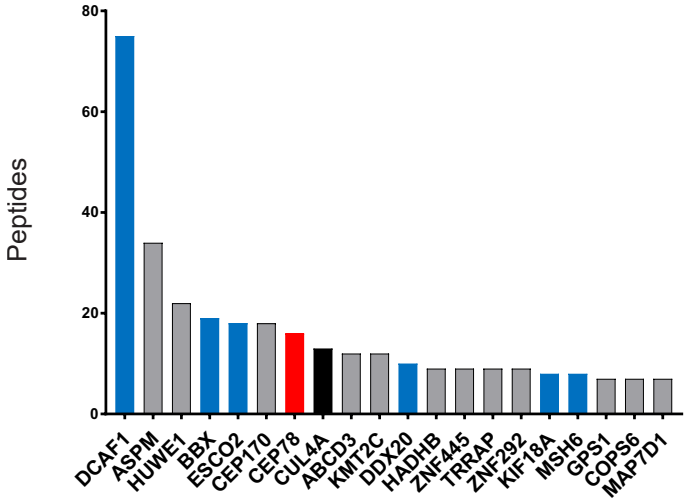

c

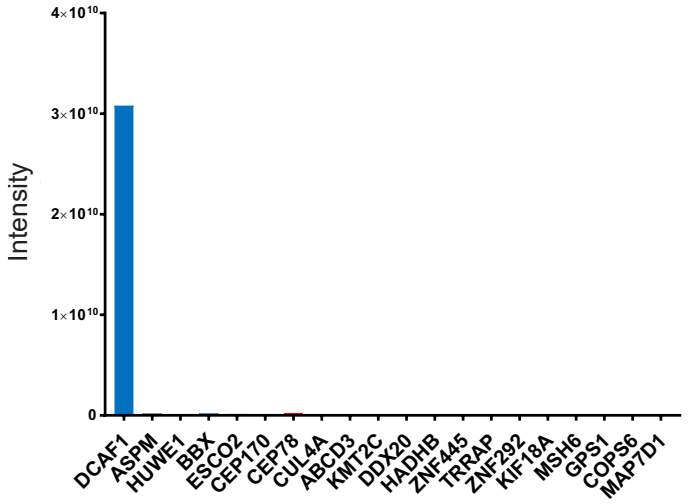

d

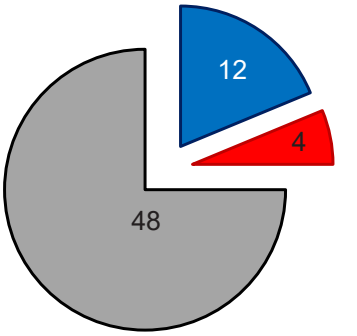

e

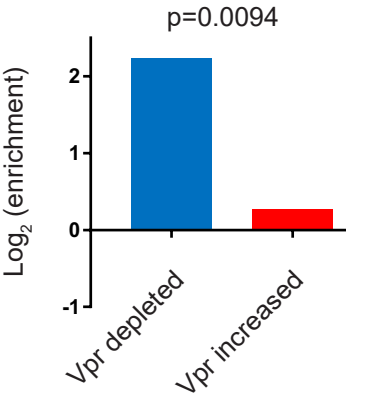

Supplementary Fig.8

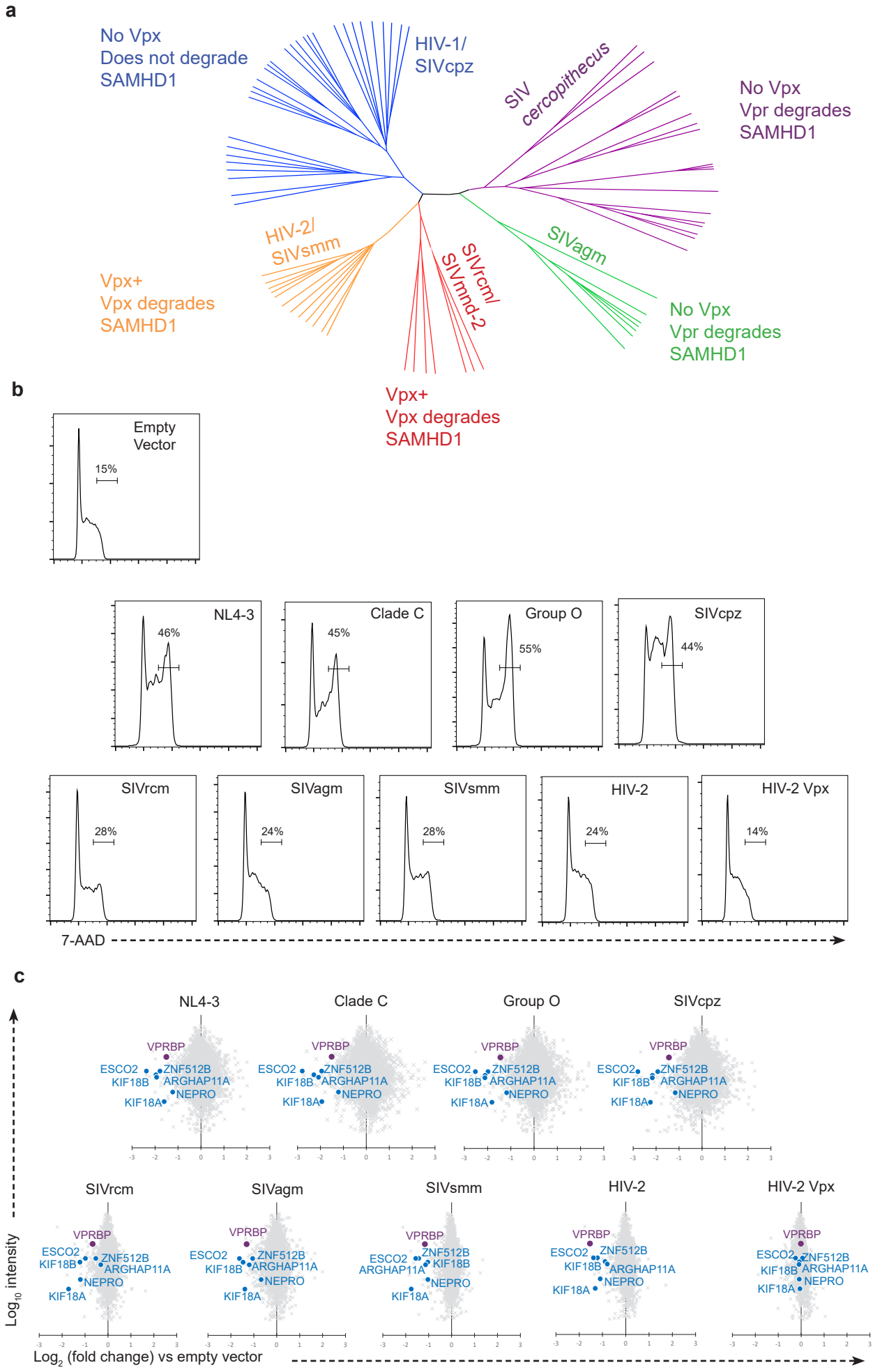

Supplementary Table 1 - example

Enter gene name here ↓
KIF18B

	Gene ID found	Single ID?	Unique peptides
WT/ΔVpr (Fig.1a)	Yes	Yes	13
VLP experiment (Fig 2a)	Yes	Yes	5
shDCAF experiment (Fig 2)	Yes	Yes	16
Pulsed SILAC 6 h (Fig.3)	Yes	Yes	8
Pulsed SILAC 24 h (Fig.3)	Yes	Yes	6
MS-IP (Supplementary Fig.7	Not found	Not found	Not found
Vpr/Vpx varients (Figure 4a)	Yes	Yes	11

Instructions and notes for use

Use this sheet to explore how indiviudal proteins of interest behave in the datasets presented in this work.

Enter the gene name of interest above and graphs will be populated on the right.

If no data is found, you may not be using the correct gene name (e.g. must enter BST2, not Tetherin or BST-2).

Proteins identified with fewer than three petpides may have less accurate quantifiction. Proteins quantified with fewer than three peptides are excluded from downstream analysis unless assayed in triplicate, but the data is included here.

Where a gene is represented by >1 UniProt ID (fragments, isoforms and variants), 'Single ID?' column above will read the number of accessions related to that gene name within that dataset- graphs will still be populated but other isoforms should be checked manually in the accompanying datasets. Number of protein isoforms, unique peptdies, and the presence and absence of proteins vary across the datasets.

Here, each Uniprot accession is associated only with a single gene name. Where a one Uniprot accession is normally associated with more than one gene, only the first gene is searchable - e.g. SMN1 and SMN2 share a uniprot accession, and are only searchable as SMN1.

WT and ΔVpr infection (Fig.1a)

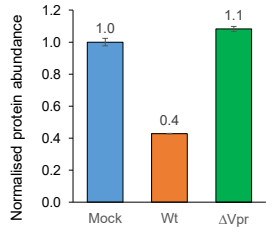

Comparison	Log2 (Fold change)	q-value
WT vs Mock	-1.22	4.1E-06
ΔVpr vs Mock	0.11	2.1E-01
WT vs ΔVpr	-1.34	4.4E-06

Viral particles (Fig. 2a)

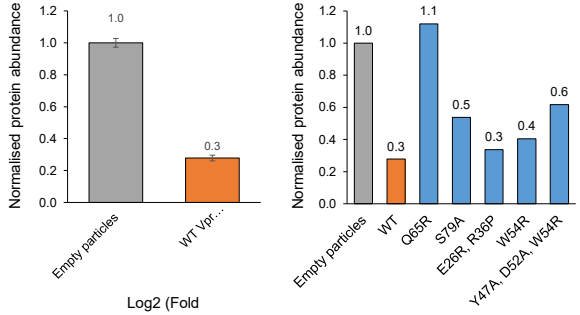

Comparison	Log2 (Fold change)	q-value
WT vs Mock	-1.84	9.6E-05

Sh-DCAF1 (Fig. 2f)

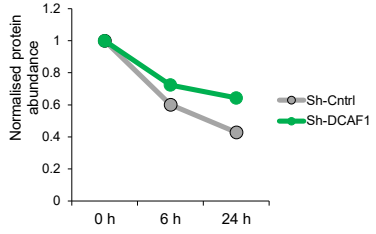

Pulsed-SILAC (Fig. 3a)

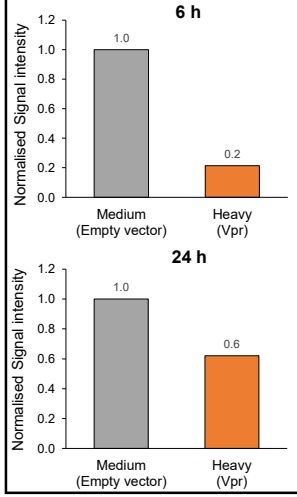

IP-MS (Supplementary Fig. 7a)

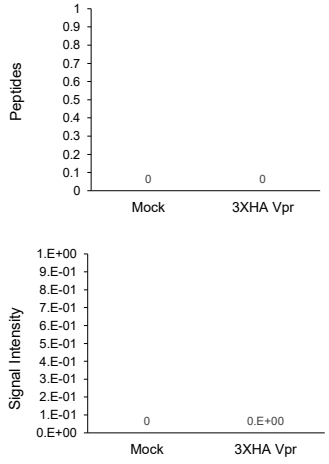

Vpr / Vpx panel, (Fig. 4a)

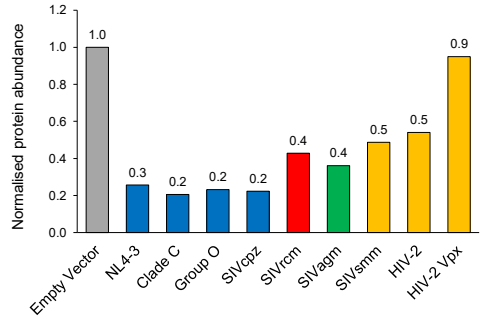

Supplementary Table 2

Accession	Gene	Vpr necessary	Incoming Vpr sufficient	Degraded within 6 h	Co-IP	In direct target list (Fig. 3d)?
Q14527	HLTF	Yes	Yes	Yes	-	Yes
Q7L590	MCM10	Yes	Yes	ND	-	No - Not detected in 6 hour pulse SILAC or IP
Q8N5A5	ZGPAT	Yes	Yes	Yes	-	Yes
Q96AY2	EME1	Yes	Yes	NS	-	No - depleted but with a Sig.B value of >0.01 in the pulsed SILAC experiment, not detected in IP
Q96NY9	MUS81	Yes	Yes	Yes	-	Yes
Q6N021	TET2	Yes	ND	ND	-	No - Not detected in incoming Vpr experiment (Fig. 2a)
P13051	UNG	Yes	Yes	NS	-	No - depleted but with a Sig.B value of >0.01 in the pulsed SILAC experiment. Detected in the Co-IP but with a single peptide

Supplementary Table 3

RNAi depletion or chemical inhibition of these Vpr depleted proteins:	Results in this Vpr associated phenotype:
ESCO2(48), **KIF18A**(49), **HASPIN**(50), **GNL3L**(51), **NUSAP1**(53), **KIF20A**(54), PHF8(55), MCM10(56), WT1(57), RECQL5(58)	Cell cycle arrest at G2/M
SMN1(60), **DDX20**(61), RIOK3(62), SENP6(63)	Enhancement/stimulation of NF-κB signalling
GNL3L(64), **CCNT1**(65), **PINX1**(66), WRN(67)	Inhibition of NF-κB signalling
ESCO2(48), **HASPIN**(68), **CDCA5**(69)	Premature chromatid segregation.

Supplementary Table 4

Vpr **Species**	**Genbank** **Accession**	**Data presented in:**
HIV-1 $_{NL4-3}$	AF324493.2(70)	All figures.
HIV-1 $_{98BR004}$ (Clade C)	AAK31002.1(71)	Proteomics experiment (Fig. 4a-d), I.B. (Fig.4e)
HIV-1 $_{BCF09}$ (Group O)	CAA75954.1	Proteomics experiment (Fig. 4a-d)
SIVcpzPtt $_{MB897}$	ABU53019.1(72)	Proteomics experiment (Fig. 4a-d), I.B. (Fig.4e)
SIVrcm $_{02CM8081}$	ADK78264.1(73)	Proteomics experiment (Fig. 4a-d), I.B. (Fig.4e)
SIVagm $_{Sab92018}$	ADO34202.1(74)	Proteomics experiment (Fig. 4a-d), I.B. (Fig.4e), I.B. (Fig. 4h)
SIVsmm $_{E660}$	ANT86736.1(75)	Proteomics experiment (Fig. 4a-d), I.B. (Fig.4e)
HIV-2 $_{ROD}$	CAA28911.1(76)	Proteomics experiment (Fig. 4a-d)
HIV-2 $_{7312a}$	AAL31354.1	I.B. (Fig.4e), I.B. (Fig. 4h)
SIVmus $_{01CM1239}$	ABO61047.1(77)	I.B. (Fig.4e), I.B. (Fig. 4h)

Vpx

Species	**Genbank** **Accession**	**Data presented in:**
HIV-2 $_{ROD}$	AAB00766.1(76)	Proteomics experiment (Fig. 4a-d)
HIV-2 $_{7312a}$	AAL31353.1	I.B. (Fig. 4h)
SIVrcm $_{Ng411}$	AAK69676.1(78)	I.B. (Fig. 4h)
SIVmnd-2$_{5440}$	AAO22477.1 (79)	I.B. (Fig. 4h)

549 **Supplementary methods**

550 **Gene ontology enrichment analysis**

551 Analysis was carried out using Panther(80), using the web interface at: http://pantherdb.org/. Lists
552 of proteins highly significantly depleted or increased by Vpr were compared to a background list of
553 proteins quantified in the two experiments used to define those lists.

554 **7-AAD staining**

555 Cells were fixed in ice cold 70% ethanol for at least 30 minutes, washed with PBS and stained in
556 25ug/ml 7-AAD for 15 minutes before acquisition on a BD FACSCalibur.

557 **Phylogenetic tree of Vif sequences.**

558 An existing nucleic acid sequence alignment of 191 representative Vif sequences from HIV-1, HIV-2
559 and SIVs from 22 primate species was downloaded from:

560 https://www.hiv.lanl.gov/content/sequence/NEWALIGN/align.html

561 A tree was generated using the percentage identity average distance in jalview(81) and visualised in
562 Figtree:

563 http://tree.bio.ed.ac.uk/software/figtree/

564 10 sequences from 5 primate species not falling into the 5 highlighted linages are not shown.

565 **Sample Preparation for Mass spectrometry**

566 Samples were prepared using three different methods depending on the experiment. Initial infection
567 experiment was by SDC-FASP. VLP and shRNA experiments were by PreOmics NHS-iST sample
568 preparation Kit. pSILAC and MS-IP experiments were by SP3.

569 *SDC-FASP*

570 Samples prepared essentially according to the protocol in Leon *et al*(82). Briefly samples were lysed
571 in 50mM TEAB (pH8.5) 2% SDS, reduced and alkylated with TCEP/Iodoacetamide, quantified by BCA
572 assay. 50ug of each sample was diluted with TEAB/8M urea for loading onto 30kDa ultrafiltration
573 devices. Samples were washed 3 times with 500uL urea buffer and 3 times with digestion buffer
574 (TEAB/0.5% sodium deoxycholate) before resuspending in 50uL digestion buffer containing 1ug
575 trypsin and incubating overnight at 37 degrees. After digestion samples were spun through the filters
576 and filters washed with 50uL TEAB. SDC was removed by acidification and two phase partitioning with
577 ethyl acetate before vacuum drying and labelling with TMT reagents according to the manufacturer's
578 instructions.

579 *PreOmics iST*

580 Samples lysed in kit lysis buffer and quantified by BCA assay. 25ug of each sample was digested
581 essentially according to manufacturer's instructions, scaling volumes for a digestion of 25ug total
582 protein.

583 *SP3*

584 Samples were lysed in 50mM TEAB (pH8.5) 2% SDS (MS-IPs were adjusted to 2% SDS), reduced and
585 alkylated with TCEP/Iodoacetamide before digestion using the SP3 method(83). Briefly, carboxylate
586 modified paramagnetic beads are added to the sample and protein is bound to the beads by
587 acidification with formic acid and addition of acetonitrile (ACN, final 50%). The beads are then washed
588 sequentially with 100% ACN, 70% Ethanol (twice) and 100% ACN. 10-20uL TEAB (Triethylammonium
589 bicarbonate) pH8 and 0.1% Sodium deoxycholate (SDC) is then added to the washed beads along with
590 trypsin. Samples were then incubated overnight at 37 degrees with periodic shaking at 2000rpm. After
591 digestion, peptides are immobilised on beads by addition of 200-400uL ACN and washed twice with
592 100uL ACN before eluting in 19uL 2% DMSO and removing the eluted peptide from the beads.

593 **Off-line high pH reversed-phase (HpRP) peptide fractionation**

594 For whole cell proteome samples HpRP fractionation was conducted on an Ultimate 3000 UHPLC
595 system (Thermo Scientific) equipped with a 2.1 mm × 15 cm, 1.7µ Aqcuity BEH C18 column (Waters,
596 UK). Solvent A was 3% ACN, Solvent B was 100% ACN, solvent C was 200 mM ammonium formate (pH
597 10). Throughout the analysis solvent C was kept at a constant 10%. The flow rate was 400 µL/min and
598 UV was monitored at 280 nm. Samples were loaded in 90% A for 10 min before a gradient elution of
599 0–10% B over 10 min (curve 3), 10-34% B over 21 min (curve 5), 34-50% B over 5 mins (curve 5)
600 followed by a 10 min wash with 90% B. 15 s (100 µL) fractions were collected throughout the run.
601 Peptide containing fractions were orthogonally recombined into 24 fractions (i.e. fractions 1, 25, 49,
602 73, 97 combined) and dried in a vacuum centrifuge. Fractions were stored at −80°C prior to analysis.

603 **Mass spectrometry**

604 Data were acquired on an Orbitrap Fusion mass spectrometer (Thermo Scientific) coupled to an
605 Ultimate 3000 RSLC nano UHPLC (Thermo Scientific). HpRP fractions were resuspended in 20 µl 5%
606 DMSO 0.5% TFA and 10uL injected. Fractions were loaded at 10 µl/min for 5 min on to an Acclaim
607 PepMap C18 cartridge trap column (300 um × 5 mm, 5 um particle size) in 0.1% TFA. After loading a
608 linear gradient of 3–32% solvent B was used for sample separation over a column of the same
609 stationary phase (75 µm × 50 cm, 2 µm particle size) before washing at 90% B and re-equilibration.
610 Solvents were A: 0.1% FA and B:ACN/0.1% FA. 3h gradients were used for whole cell proteomics
611 samples, 1h gradients for MS-IPs.

612 An SPS/MS3 acquisition was used for TMT experiments and was run as follows. MS1: Quadrupole
613 isolation, 120’000 resolution, 5e5 AGC target, 50 ms maximum injection time, ions injected for all
614 parallelisable time. MS2: Quadrupole isolation at an isolation width of m/z 0.7, CID fragmentation
615 (NCE 35) with the ion trap scanning out in rapid mode from m/z 120, 8e3 AGC target, 70 ms maximum
616 injection time, ions accumulated for all parallelisable time. In synchronous precursor selection mode
617 the top 10 MS2 ions were selected for HCD fragmentation (65NCE) and scanned out in the orbitrap at
618 50’000 resolution with an AGC target of 2e4 and a maximum accumulation time of 120 ms, ions were
619 not accumulated for all parallelisable time. The entire MS/MS/MS cycle had a target time of 3s.
620 Dynamic exclusion was set to +/−10 ppm for 90 s, MS2 fragmentation was trigged on precursor ions
621 5e3 counts and above. For MS-IPs, MS2 instead used HCD fragmentation (NCE 34) and a maximum
622 injection time of 250ms and had a target cycle time of 2s. For pSILAC MS1 was acquired at 240’000
623 resolution.

624 **Data processing and analysis**

625 For TMT labelled samples data were searched by Mascot within Proteome Discoverer 2.1 in two
626 rounds of searching. First search was against the UniProt Human reference proteome (26/09/17), the
627 HIV proteome and compendium of common contaminants (GPM). The second search took all
628 unmatched spectra from the first search and searched against the human trEMBL database (Uniprot,
629 26/09/17). The following search parameters were used. MS1 Tol: 10 ppm, MS2 Tol: 0.6 Da. Enzyme:
630 Trypsin (/P). MS3 spectra were used for reporter ion based quantitation with a most confident
631 centroid tolerance of 20 ppm. PSM FDR was calculated using Mascot percolator and was controlled at
632 0.01% for 'high' confidence PSMs and 0.05% for 'medium' confidence PSMs. Normalisation was
633 automated and based on total s/n in each channel. Protein/peptide abundance was calculated and
634 output in terms of 'scaled' values, where the total s/n across all reporter channels is calculated and a
635 normalised contribution of each channel is output. Proteins/peptides satisfying at least a 'medium'
636 FDR confidence were taken forth to statistical analysis in R. This consisted of a moderated T-test
637 (Limma) with Benjamini-Hochberg correction for multiple hypotheses to provide a q value for each
638 comparison(84). MS-IPs were submitted to a similar search workflow with quantitative data being
639 derived from MS1 spectra via proteome discover minora feature detector node. For pSILAC
640 experiments data were processed in MaxQuant and searched using Andromeda with similar search
641 parameters(85). MaxQuant output was uploaded into Perseus for calculation of significance B(86).
642 Where conditions were not carried out in triplicate, downstream analysis was limited to proteins
643 identified with at least 3 unique peptides.

644

645 **Supplementary References**

646

647 48. Hou F & Zou H (2005) Two human orthologues of Eco1/Ctf7 acetyltransferases are both
648 required for proper sister-chromatid cohesion. *Mol Biol Cell* 16(8):3908-3918.
649 49. Mayr MI*, et al.* (2007) The human kinesin Kif18A is a motile microtubule depolymerase
650 essential for chromosome congression. *Curr Biol* 17(6):488-498.
651 50. Huertas D*, et al.* (2012) Antitumor activity of a small-molecule inhibitor of the histone kinase
652 Haspin. *Oncogene* 31(11):1408-1418.
653 51. Meng L, Hsu JK, & Tsai RY (2011) GNL3L depletion destabilizes MDM2 and induces p53-
654 dependent G2/M arrest. *Oncogene* 30(14):1716-1726.
655 52. Kinor N & Shav-Tal Y (2011) The dynamics of the alternatively spliced NOL7 gene products
656 and role in nucleolar architecture. *Nucleus* 2(3):229-245.
657 53. Gordon CA, Gong X, Ganesh D, & Brooks JD (2017) NUSAP1 promotes invasion and
658 metastasis of prostate cancer. *Oncotarget* 8(18):29935-29950.
659 54. Kawai Y*, et al.* (2018) KIF20A expression as a prognostic indicator and its possible
660 involvement in the proliferation of ovarian clearcell carcinoma cells. *Oncol Rep* 40(1):195-
661 205.
662 55. Lim HJ*, et al.* (2013) The G2/M regulator histone demethylase PHF8 is targeted for
663 degradation by the anaphase-promoting complex containing CDC20. *Mol Cell Biol*
664 33(21):4166-4180.
665 56. Park JH, Bang SW, Kim SH, & Hwang DS (2008) Knockdown of human MCM10 activates G2
666 checkpoint pathway. *Biochem Biophys Res Commun* 365(3):490-495.
667 57. Yamagami T*, et al.* (1998) Suppression of Wilms' tumor gene (WT1) expression induces
668 G2/M arrest in leukemic cells. *Leuk Res* 22(4):383-384.
669 58. Ramamoorthy M*, et al.* (2012) RECQL5 cooperates with Topoisomerase II alpha in DNA
670 decatenation and cell cycle progression. *Nucleic Acids Res* 40(4):1621-1635.

671 59. Yin T*, et al.* (2014) A novel CDK9 inhibitor shows potent antitumor efficacy in preclinical
672 hematologic tumor models. *Mol Cancer Ther* 13(6):1442-1456.
673 60. Kim EK & Choi EJ (2017) SMN1 functions as a novel inhibitor for TRAF6-mediated NF-kappaB
674 signaling. *Biochim Biophys Acta* 1864(5):760-770.
675 61. Takata A*, et al.* (2012) A miRNA machinery component DDX20 controls NF-kappaB via
676 microRNA-140 function. *Biochem Biophys Res Commun* 420(3):564-569.
677 62. Shan J*, et al.* (2009) RIOK3 interacts with caspase-10 and negatively regulates the NF-kappaB
678 signaling pathway. *Mol Cell Biochem* 332(1-2):113-120.
679 63. Liu X, Chen W, Wang Q, Li L, & Wang C (2013) Negative regulation of TLR inflammatory
680 signaling by the SUMO-deconjugating enzyme SENP6. *PLoS Pathog* 9(6):e1003480.
681 64. Thoompumkal IJ, Rehna K, Anbarasu K, & Mahalingam S (2016) Leucine Zipper Down-
682 regulated in Cancer-1 (LDOC1) interacts with Guanine nucleotide binding protein-like 3-like
683 (GNL3L) to modulate Nuclear Factor-kappa B (NF-kappaB) signaling during cell proliferation.
684 *Cell Cycle* 15(23):3251-3267.
685 65. Ramakrishnan R*, et al.* (2012) Identification of novel CDK9 and Cyclin T1-associated protein
686 complexes (CCAPs) whose siRNA depletion enhances HIV-1 Tat function. *Retrovirology* 9:90.
687 66. Deacon K & Knox AJ (2018) PINX1 and TERT Are Required for TNF-alpha-Induced Airway
688 Smooth Muscle Chemokine Gene Expression. *J Immunol* 200(4):1283-1294.
689 67. Mizutani T, Ishizaka A, & Furuichi Y (2015) The Werner Protein Acts as a Coactivator of
690 Nuclear Factor kappaB (NF-kappaB) on HIV-1 and Interleukin-8 (IL-8) Promoters. *J Biol Chem*
691 290(30):18391-18399.
692 68. Dai J, Sullivan BA, & Higgins JM (2006) Regulation of mitotic chromosome cohesion by
693 Haspin and Aurora B. *Dev Cell* 11(5):741-750.
694 69. Rankin S, Ayad NG, & Kirschner MW (2005) Sororin, a substrate of the anaphase-promoting
695 complex, is required for sister chromatid cohesion in vertebrates. *Mol Cell* 18(2):185-200.
696 70. Adachi A*, et al.* (1986) Production of acquired immunodeficiency syndrome-associated
697 retrovirus in human and nonhuman cells transfected with an infectious molecular clone.
698 *Journal of virology* 59(2):284-291.
699 71. Rodenburg CM*, et al.* (2001) Near full-length clones and reference sequences for subtype C
700 isolates of HIV type 1 from three different continents. *AIDS Res Hum Retroviruses* 17(2):161-
701 168.
702 72. Van Heuverswyn F*, et al.* (2007) Genetic diversity and phylogeographic clustering of
703 SIVcpzPtt in wild chimpanzees in Cameroon. *Virology* 368(1):155-171.
704 73. Ahuka-Mundeke S*, et al.* (2010) Full-length genome sequence of a simian immunodeficiency
705 virus (SIV) infecting a captive agile mangabey (Cercocebus agilis) is closely related to SIVrcm
706 infecting wild red-capped mangabeys (Cercocebus torquatus) in Cameroon. *The Journal of*
707 *general virology* 91(Pt 12):2959-2964.
708 74. Gnanadurai CW*, et al.* (2010) Genetic identity and biological phenotype of a
709 transmitted/founder virus representative of nonpathogenic simian immunodeficiency virus
710 infection in African green monkeys. *Journal of virology* 84(23):12245-12254.
711 75. Lopker MJ*, et al.* (2016) Derivation and Characterization of Pathogenic Transmitted/Founder
712 Molecular Clones from Simian Immunodeficiency Virus SIVsmE660 and SIVmac251 following
713 Mucosal Infection. *Journal of virology* 90(19):8435-8453.
714 76. Guyader M*, et al.* (1987) Genome organization and transactivation of the human
715 immunodeficiency virus type 2. *Nature* 326(6114):662-669.
716 77. Aghokeng AF*, et al.* (2007) Full-length sequence analysis of SIVmus in wild populations of
717 mustached monkeys (Cercopithecus cephus) from Cameroon provides evidence for two co-
718 circulating SIVmus lineages. *Virology* 360(2):407-418.
719 78. Beer BE*, et al.* (2001) Characterization of novel simian immunodeficiency viruses from red-
720 capped mangabeys from Nigeria (SIVrcmNG409 and -NG411). *Journal of virology*
721 75(24):12014-12027.

722 79. Hu J*, et al.* (2003) Characterization and comparison of recombinant simian
723 immunodeficiency virus from drill (Mandrillus leucophaeus) and mandrill (Mandrillus sphinx)
724 isolates. *Journal of virology* 77(8):4867-4880.
725 80. Mi H*, et al.* (2017) PANTHER version 11: expanded annotation data from Gene Ontology and
726 Reactome pathways, and data analysis tool enhancements. *Nucleic acids research*
727 45(D1):D183-D189.
728 81. Waterhouse AM, Procter JB, Martin DM, Clamp M, & Barton GJ (2009) Jalview Version 2--a
729 multiple sequence alignment editor and analysis workbench. *Bioinformatics* 25(9):1189-
730 1191.
731 82. Leon IR, Schwammle V, Jensen ON, & Sprenger RR (2013) Quantitative assessment of in-
732 solution digestion efficiency identifies optimal protocols for unbiased protein analysis. *Mol*
733 *Cell Proteomics* 12(10):2992-3005.
734 83. Hughes CS*, et al.* (2014) Ultrasensitive proteome analysis using paramagnetic bead
735 technology. *Mol Syst Biol* 10:757.
736 84. Schwammle V, Leon IR, & Jensen ON (2013) Assessment and improvement of statistical tools
737 for comparative proteomics analysis of sparse data sets with few experimental replicates. *J*
738 *Proteome Res* 12(9):3874-3883.
739 85. Cox J & Mann M (2008) MaxQuant enables high peptide identification rates, individualized
740 p.p.b.-range mass accuracies and proteome-wide protein quantification. *Nat Biotechnol*
741 26(12):1367-1372.
742 86. Tyanova S*, et al.* (2016) The Perseus computational platform for comprehensive analysis of
743 (prote)omics data. *Nat Methods* 13(9):731-740.

744